ACS OMEGA

Article

Cite This: ACS Omega 2018, 3, 9126−9145

http://pubs.acs.org/journal/acsodf

Multifunctional Carbon-Based Nanomaterials: Applications in Biomolecular Imaging and Therapy

Yanyan Zhang,[†,#] Minghao Wu,[‡,#] Mingjie Wu,[§,#] Jingyi Zhu,[∥] and Xuening Zhang*[,†]

[†]Department of Medical Imaging, Second Hospital of Tianjin Medical University, Tianjin 300211, P. R. China

[‡]Department of Radiology, Tianjin Medical University Cancer Institute and Hospital, National Clinical Research Center for Cancer, Tianjin's Clinical Research Center for Cancer Key Laboratory of Cancer Prevention and Therapy, Tianjin 300060, P. R. China

[§]Institut National de la Recherche Scientifique-Énergie Matériaux et Télécommunications, Varennes, Quebec J3X 1S2, Canada

[∥]School of Pharmaceutical Science, Nanjing Tech University, Nanjing 211816, P. R. China

ABSTRACT: Molecular imaging has been widely used not only as an important detection technology in the field of medical imaging for cancer diagnosis but also as a theranostic approach for cancer in recent years. Multifunctional carbon-based nanomaterials (MCBNs), characterized by unparalleled optical, electronic, and thermal properties, have attracted increasing interest and demonstrably hold the greatest promise in biomolecular imaging and therapy. As such, it should come as no surprise that MCBNs have already revealed a great deal of potential applications in biomedical areas, such as bioimaging, drug delivery, and tumor therapy. Carbon nanomaterials can be categorized as graphene, single-walled carbon nanotubes, mesoporous carbon, nanodiamonds, fullerenes, or carbon dots on the basis of their morphologies. In this article, reports of the use of MCBNs in various chemical conjugation/functionalization strategies, focusing on their applications in cancer molecular imaging and imaging-guided therapy, will be comprehensively summarized. MCBNs show the possibility to serve as optimal candidates for precise cancer biotheranostics.

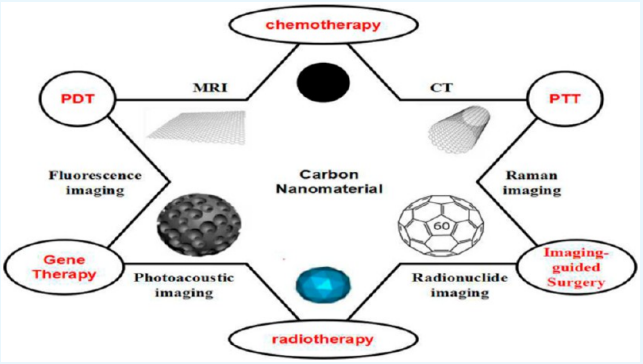

1. INTRODUCTION

Molecular imaging plays a crucial role in early accurate diagnosis and therapy for 21st-century cancer management.[1] Recently, inorganic nanomaterials (gold nanoparticles, iron oxide nanoparticles, silica nanoparticles, carbon nanoparticles, etc.) with various unique intrinsic physical properties have attracted tremendous interest in cancer theranostic (i.e., combined diagnostic and therapeutic) applications.[2−6] To this end, carbon-based nanoparticles have shown great promise as the next generation of theranostic probes due to their excellent mechanical, thermal, and optical properties (Figure 1).[7,8] Carbon nanoparticles are mainly categorized as graphene, single-walled carbon nanotubes, mesoporous carbon, nanodiamonds, fullerenes, or carbon dots.[9,10]

1.1. Graphene. Graphene family nanomaterials (GFNs), without question, are the most extensively studied materials by virtue of their great number of extraordinary physicochemical properties.[7,11,12] As the world's strongest, thinnest, and stiffest materials,[11] GFNs are characterized by alluring optical characteristics (e.g., the ability to quench fluorescence),[13] a large specific planar surface area (2630 m^2 g^{-1}),[14] and unparalleled thermal conductivity (5000 W m^{-1} K^{-1}).[15] GFNs are distinguished mainly on the basis of various chemical modifications and include graphene, graphene oxide (GO), and reduced graphene oxide (rGO) (Figure 2).[7,16,17]

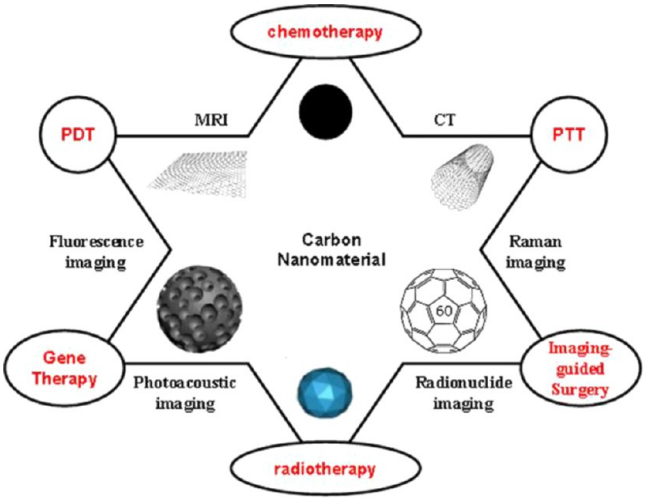

Figure 1. Schematic illustration of theranostic applications of carbon nanomaterials in cancer.

Received: May 21, 2018
Accepted: July 27, 2018
Published: August 15, 2018

DOI: 10.1021/acsomega.8b01071
ACS Omega 2018, 3, 9126−9145

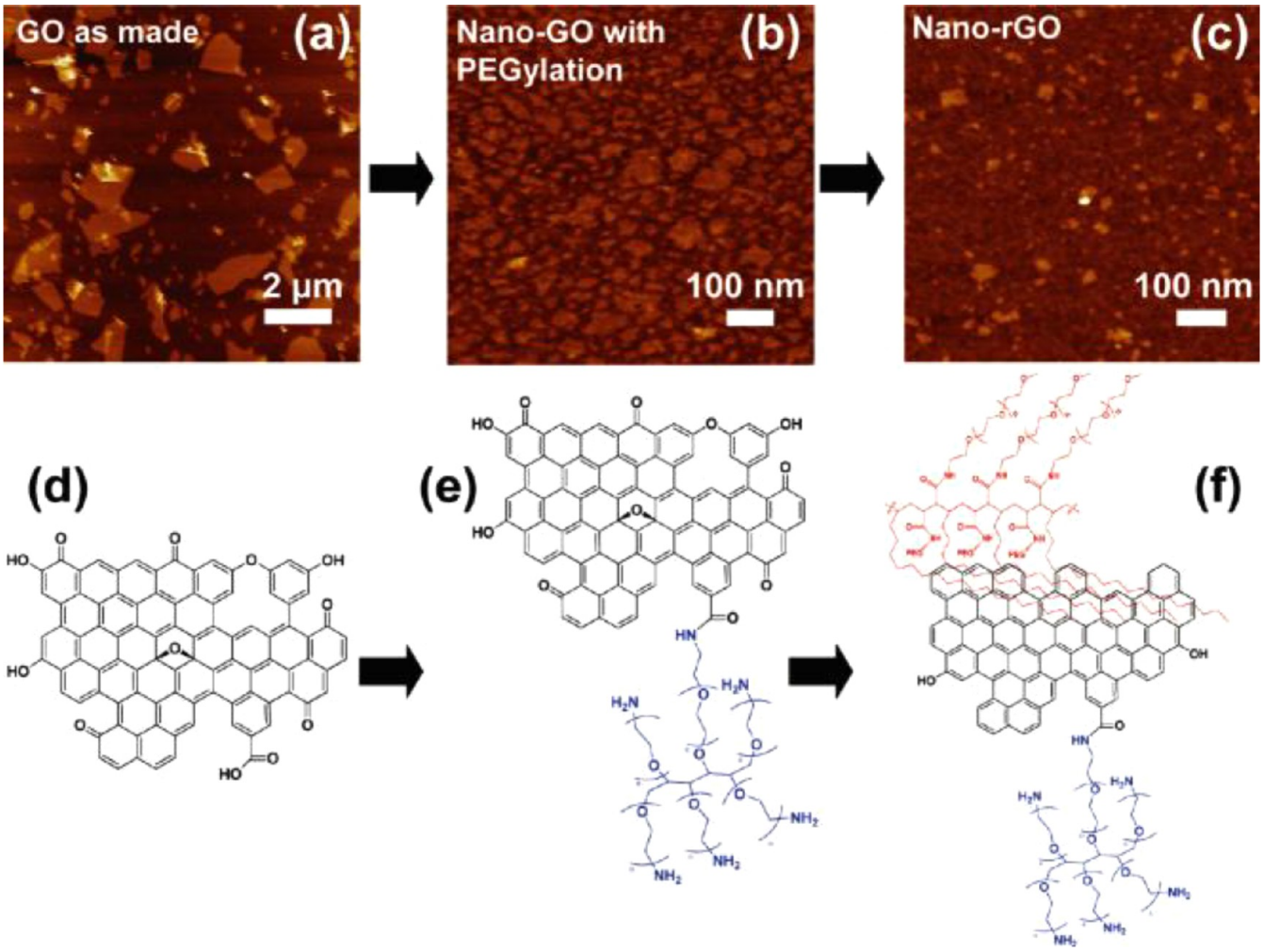

Figure 2. (a) AFM image of as-made graphene oxide (GO). (b) AFM of covalently PEGylated nanographene oxide (nano-GO). (c) AFM of reduced nanographene oxide (nano-rGO). All images are on a 10 nm height scale. (d–f) Schematic drawings of (d) as-made GO, (e) nano-GO, and (f) nano-rGO illustrating the reaction steps. Reprinted with permission from ref 17. Copyright 2011 American Chemical Society.

Wherein defect-free graphene is not commonly used due to the difficulty of its bulk synthesis, it can be suspended in solutions and isolated in the gas phase on account of its highly reactive surface, so GO and rGO are widely applied in biomedical areas. GO, a highly oxidized form of chemically modified graphene, has many distinct characteristics resulting from the presence of numerous oxygen-containing hydroxyl groups, carboxylic acids, and epoxides in the plane.[7,18] In terms of its benefits, GO possesses colloidal stability and allows surface modification.[9,19] Moreover, with the presence of the free surface π electrons from unoxidized areas of graphene enabling hydrophobic properties, drug loading by $\pi-\pi$ interactions, and non-covalent functionalization, GO can serve as a surfactant to stabilize hydrophobic molecules in solution.[20] Recent research has demonstrated that GO can be functionalized by biomolecules (e.g., proteins, peptides, small organic molecules, etc.) to enhance unique physicochemical properties required for specific applications when compared to the use of either material alone. For example, Zhang et al. functionalized GO with folic acid (FA) as a cancer-targeting molecule and loaded doxorubicin (DOX) and camptothecin onto the large surface area of GO via $\pi-\pi$ stacking.[21] Compared with GO, rGO, characterized by lower oxygen content, weaker surface charge, and poorer hydrophilicity, is capable of higher light absorption in the visible and infrared regions.[17,22−24] This is because the chemical reduction restored part of the disrupted π conjugation from highly oxidized GO.[17] As a result, functionalized graphene composite nanomaterials are powerful driving forces in the field of bioapplications.

1.2. Single-Walled Carbon Nanotubes (SWNTs). Since the discovery of carbon nanotubes by Iijima in 1991,[25] they have been rapidly developed as a platform for biomedical applications.[26] SWNTs are cylindrical and sp^2-hybridized carbon nanomaterials with nanometer-scale diameters 100−1000 times less than their length, resulting in very large aspect ratios.[6,27] Owing to their unique structure, SWNTs exhibit intrinsic optical properties (i.e., strong resonant Raman scattering[28] and photoluminance in the near-infrared (NIR) range)[29,30] that have potential for implementation in bioimaging.[31−35] However, composites incorporating SWNTs have not yet been proven to be competent theranostic agents, mostly because of their poor interaction with the surrounding matrices, leading to inefficient loading ratio and instability.[9] Therefore, many recent research efforts have been focused on functionalization of SWNTs for bioimaging, ranging from single-modal imaging[29] to multimodal imaging,[36] and even imaging-guided chemo-photothermal therapy.[37,38] By combining these unique and robust nanomaterials, SWNT−nano-

DOI: 10.1021/acsomega.8b01071
ACS Omega 2018, 3, 9126−9145

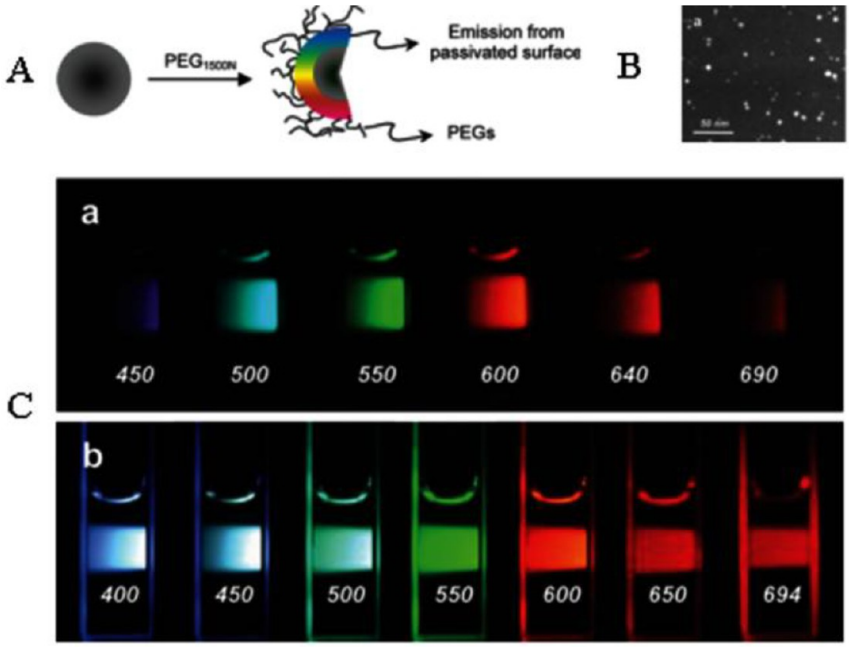

Figure 3. (A) Surface passivation by attaching simple organic species to acid-treated carbon dots. (B) Representative STEM images of carbon dots surface-passivated with PEG1500N. (C) Photograph of the PEG1500N-attached carbon dots solution (a) excited at 400 nm under band-pass filters of different wavelengths as indicated and (b) excited at the indicated wavelengths directly. Reprinted with permission from ref 60. Copyright 2006 American Chemical Society.

particle hybrid structures give access not only to the individual properties of the nanoparticles but to additional superiorities, such as remarkable biocompatibility and synergistic properties.

1.3. Mesoporous Carbon Nanoparticles (MCNs). Mesoporous nanoparticles, especially mesoporous silica-based nanoparticles (MSNs), have been applied in the fields of biotechnology and nanomedicine due to their high surface area, large pore volume, and uniform mesoporous structures.[39−44] However, MSNs have severe drawbacks, such as tedious surface modification processes,[39] low loading capacity,[45] and potential toxicity for in vivo applications.[46−48] As such, it is continuously a hot topic to construct an intelligent nanoporous platform with simultaneous controlled drug release and diagnostic imaging performance.[39] As the newcomers to the carbon-based family of compounds in nanomedicine, three-dimensional mesoporous carbon nanoparticles (MCNs) with pore size in the range 2−50 nm are leading theranostic materials because of their well-defined nanoporous structures, high pore volume, and high biocompatibility.[39,48−53] Specifically, MCNs-based intelligent multifunctional composite nanosystems have gradually emerged at the foreground of bioapplications, especially for serving as intelligent theranostic platforms for stimuli-responsive drug delivery and molecular imaging.[39,49]

1.4. Carbon Dots (CDs). Nanoscale carbon particles (carbon dots, or CDs), a recently discovered class of carbon nanomaterials, have drawn much attention due to their unique properties, such as excellent water solubility and excellent biocompatibility.[54−58] Recently, surface-passivated CDs have been reported to exhibit strong photoluminescence (PL), with spectral features and properties in the visible spectrum (Figure 3).[59,60] CDs that exhibit bright photoluminescence in the visible region are characterized by two distinctive features: (1) small size (sub-10 nm) and (2) surface passivation.[59,60] Compared with conventional organic dyes and semiconductor quantum dots (QDs), CDs possess excellent fluorescence properties, such as high photostability, broad excitation spectra, and tunable emission spectra.[59,61,62] Therefore, CDs have received special attention in potential applications such as bioimaging and drug delivery.

1.5. Other Carbon-Based Nanomaterials. Nanodiamonds (NDs), referring to an octahedral architecture ranging from 5 to 50 nm in size, have seen significant progress in their development as promising candidates for molecular theranostic applications[63−65] due to their exceptional biocompatibility, easy functionalization versatility, high adsorption capacity, and thermal properties.[6,66−68] NDs can produce PL with emission in the red and NIR spectral regions (575−750 nm) and do not bring about photoquenching,[69,70] which typically results from nitrogen vacancy color centers embedded in a diamond matrix.[71,72] In addition to fluorescence properties, NDs also give access to magnetic properties because of their facet-specific electrostatics.[73] Moreover, NDs can serve as promising drug carriers due to their unique surface electrostatics.[74] With the above-mentioned electrochemical and optical properties, NDs' surfaces can be functionalized to achieve synergistic effects with fluorescent molecules,[75−77] DNA,[78] siRNA,[79] proteins,[80,81] lysozyme,[82] growth hormone,[83] cytochrome *c*,[84] alcohol dehydrogenase,[85] antibodies,[86,87] anti-cancer drugs,[74,88] and dopamine derivatives.[89,90] As such, developing NDs for future theranostic applications has extensive prospects.[91]

Fullerenes (C_{60}), soccer-ball-shaped molecules composed of 12 pentagons formed by C_5-C_5 single bonds and 20 hexagons formed by C_5-C_6 double bonds, have been widely studied since their discovery in 1985.[92−95] Subsequently, numerous fullerenes with other carbon numbers (e.g., C_{70}, C_{76}, C_{80}, and so on) have been produced,[96−98] wherein the condensed aromatic rings present in the C_{60} result in an extended π-conjugated system of molecular orbitals which produce

DOI: 10.1021/acsomega.8b01071
ACS Omega 2018, 3, 9126−9145

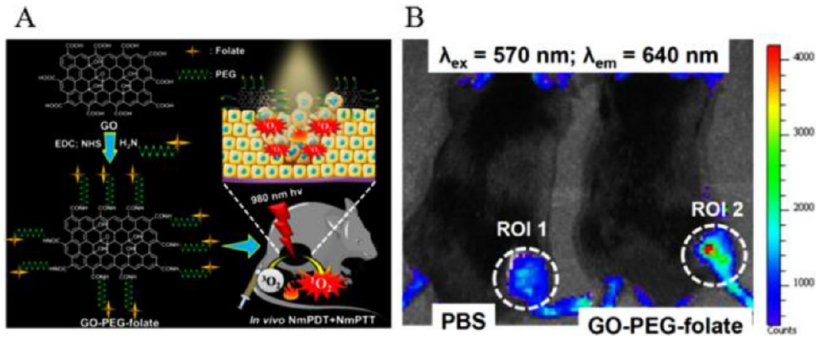

Figure 4. (A) Schematic illustration of the preparation of GO-PEG-folate to facilitate the combination of nanomaterial-mediated photothermal and photodynamic therapeutic destruction of tumors. (B) In vivo fluorescence imaging from PBS (left) and GO-PEG-folate (right) mice at 24 h after intravenous injection. Reprinted from ref 107. Copyright 2016 Elsevier Ltd.

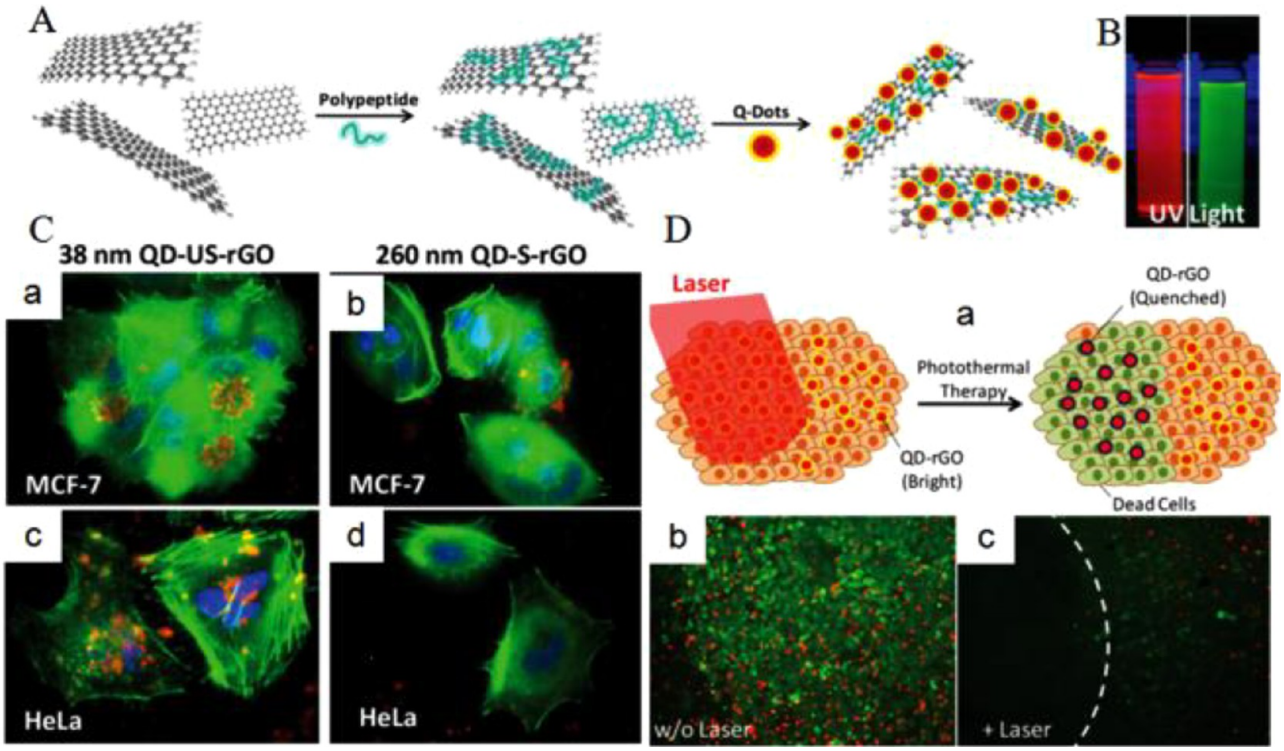

Figure 5. (A) Schematic representation of the synthesis of QD-rGO. (B) Fluorescence of the QD-tagged 38 nm rGO and the QD-tagged 260 nm rGO. (C) Cellular uptake of FA-QD-US-rGO. (D) Schematic illustration of QD-rGO under irradiation that causes cell death and diminished QD fluorescence (a) and images before (b) and after (c) irradiation. Reprinted with permission from ref 110. Copyright 2012 Wiley-VCH Verlag GmbH & Co. KGaA.

significant absorption of visible light.[99,100] With the absorption of visible light and efficient intersystem crossing to a long-lived triplet state, fullerenes can generate reactive oxygen species upon illumination and so give access to photosensitizers (PSs).[101,102] Recently, functionalized C_{60} has been realized by covalent attachment with various groups (e.g., −OH, $-NH_2$, −COOH) to make more promising candidates for theranostic applications.[93,101]

In this article, we will systematically discuss the above-described carbon-based nanomaterials in terms of their functionalization, characterization, and implementation for a host of theranostic applications. While there are already numerous excellent reviews focusing on carbon-based nanomaterials' imaging and cargo delivery, the molecular imaging and imaging-guided therapy applications of carbon-based nanomaterials have not been comprehensively reviewed. Moreover, we present the first of effort to combine MCNs with other carbon-based nanomaterials for perfect carbon-based nanomaterials. This will be followed by an in-depth analysis of the various carbon-based nanomaterials that have been developed for theranostic applications.

2. THERANOSTIC APPLICATION OF MULTIFUNCTIONAL CARBON-BASED NANOMATERIALS

2.1. Graphene. *2.1.1. Fluorescence Imaging and Therapy.* In theoretical and experimental studies, small graphene (less than 10 nm) can be used as QDs, which can be realized by reducing the connectivity of the π-electron network to induce a band gap using physical or chemical methods.[103] Recently, graphene quantum dots (GQDs) have attracted increasing interest for implementation into bioimag-

DOI: 10.1021/acsomega.8b01071
ACS Omega 2018, 3, 9126−9145

ing applications.[104] As has been reported by Zhu et al., GQDs with strong green fluorescence have been synthesized via a one-step solvothermal method for cellular imaging.[105] In addition, GQDs were explored to serve as a new generation of photodynamic therapy (PDT) agents.[106] The new agents overcame the limitations of conventional agents, such as low singlet oxygen quantum yields, photobleaching, and poor biocompatibility. Although GQDs produced a very high singlet O_2 quantum yield, this situation was attained only in the visible light region and can only offer treatment of near-skin tumors but not deeply buried tumors. Given these findings, Kalluru et al. successfully assembled a novel NIR-light-activatable theranostic platform based on GQDs (Figure 4A).[107] It was demonstrated that nano-GO-PEG-FA sensitized the generation of singlet O_2 to mediate bimodal PDT and photothermal therapy (PTT) effects on effective damage to solid tumors even in deep tissues under ultra-low laser doses of NIR light excitation. Moreover, nano-GO-PEG-FA can exhibit wavelength-dependent PL under NIR light excitation, so it is suitable for in vivo deep fluorescence imaging (Figure 4B). In view of these advantages, more GQDs-based theranostic platforms will be widely explored for fluorescence-guided therapy.

In addition to serving as QDs, graphene can also act as a carrier for other QDs or dyes to reduce their adverse effects and enhance their properties. As such, a great number of studies on dye/QDs-labeled graphene nanocomposites for fluorescence imaging have also been conducted. On one hand, Gao et al. developed a thermo-activatable hybrid nanocomplex, called CPGA, by conjugating a NIR dye (Cy5.5)-labeled matrix metalloproteinase-14 (MMP-14) substrate (CP) onto the GO/Au complex (GA),[108] wherein the Cy5.5 fluorescent signal is quenched by surface plasmon resonance (SPR) capacity from GA, yet it can boost stronger fluorescence signals after separation from GA. Compared to the other activatable fluorescent probes, CPGA had prominent quenching efficiency (95%), which gives it remarkable promise for future development of intelligent nanoplatforms. In another study, Cy5.5-labeled molecular beacon (MB) was conjugated onto GO by $\pi-\pi$ stacking interactions for highly sensitive detection and imaging of miRNAs.[109] GO can induce efficient fluorescence quenching of the dyes on MB. When the Cy5.5-MB target molecule reacted with the miRNAs to form a duplex, it was released from the GO surface and restored the fluorescence of one dye molecule in living cells and in vivo. On the other hand, to prevent fluorescence quenching, Hu et al. used a surfactant coating method to synthesize a hybrid nanocomposite of core−shell CdSe/ZnS QDs and rGO.[110] In addition to reducing the toxicity of QDs, the nanocomposite also preserved thier fluorescence characteristics by maintaining a suitable spacer between the QDs and rGO (Figure 5). Meanwhile, the QDs also acted as an optical indicator for the PTT effect by degradation resulting from the thermal effect on the irradiated rGO.

2.1.2. Raman Imaging and Therapy. Raman scattering is a photon scattering process in which photons' emission wavelengths are shifted under light excitation rather than PL.[111−113] When the laser energy reaches the desired value, required for electron transition from the valence band to the conduction band, the generated signal reflects "resonance Raman scattering".[114,115] Typically, GO can be characterized by Raman spectroscopy on the basis of its distinctive Raman spectra (D band at 1350 cm^{-1} and G band at 1600 cm^{-1}).[116] However, the inherent Raman scattering signals of GO itself are usually weak. Recently, GO was modified with noble metals (e.g., Au and Ag) to promote its Raman intensity and sensitivity, which is referred to as surface-enhanced Raman scattering (SERS).[116,117] Liu et al. decorated Au/GO hybrids that could serve as a flexible Raman probe for bioimaging applications through Raman mapping.[112] Compared to the original GO, the Raman intensity of the Au/GO hybrids was remarkably enhanced 4-fold as a consequence of the surface enhancement effect of the AuNPs. Similar results were demonstrated by other researchers.[118] Moreover, SERS shows ultrasensitivity and quantitative abilities in monitoring drug release behaviors due to its advantage of narrow spectral bands, which overcome the drawbacks of the fluorescence-traceable nanocarriers for tracking intracellular drug release dynamics.[119]

2.1.3. Magnetic Resonance Imaging (MRI) and Therapy. MRI contrast agents can reduce the T_1 and/or T_2 relaxation times of protons to enhance the magnetic resonance signal.[120] However, the conventionally used Gd^{3+}-based T_1 contrast agents have some limitations, such as short half-life, low sensitivity, nephrogenic systemic fibrosis, and renal failure.[121,122] In this regard, Gd-based nanostructures have been extensively studied to increase T_1 relaxivities and reduce safety concerns. Two-dimensional graphene serving as a carrier has attracted a great deal of attention owing to its unique physicochemical properties. Zhang et al. developed a theranostic agent based on GO-Gd complexes.[123] In this case, diethylenetriaminepentaacetic acid (DTPA) was covalently conjugated with GO, followed by Gd^{3+} complexation, resulting in formation of GO-DTPA-Gd. Next, DOX and either an anti-cancer drug or a fluorescent dye was loaded on the surface of GO via $\pi-\pi$ interactions for integrating imaging and intelligent pH-sensitive drug delivery. The agent exhibited much better contrast enhancement than the traditional Magnevist brand MRI contrast agent. Moreover, after being uptaken by cancer cells, the DOX on GO-DTPA-Gd complexes was successfully released to achieve accurate chemotherapy.

In recent years, magnetic nanoparticles (MNPs), such as Fe_2O_3 and Fe_3O_4, have been proven to possess unique magnetic properties offering sufficient sensitivity for T_2-weighted imaging.[124] In addition, suitable aggregation of MNPs has been reported to increase relaxivity rates (r_2).[125] However, uncontrolled aggregation of iron oxide nanoparticles (IONPs) can cause precipitation of the nanoparticles and thus reduce their time of circulation in the blood due to reticuloendothelial system (RES) clearance.[126] Recently, magnetic Fe_3O_4/GO complexes were employed to realize a multifunctional theranostic platform. For example, Wang et al. synthesized a multifunctional nanocarrier system based on magnetic Fe_3O_4/GO nanocomposites via inverse chemical co-precipitation.[127] This system has difunctional characteristics, with excellent MRI and intelligent pH-sensitive drug delivery.

In order to further optimize the theranostic platform, Wang et al. developed a targeting peptide-modified mesoporous silica with magnetic graphene.[128] This type of composite possesses many unique properties, such as large T_2 relaxation rates (r_2), facile magnetic separation, high NIR photothermal heating, high DOX loading capacity, and laser-mediated/pH-dependent synergistic release behavior, which make it a robust platform for cancer theranostics.

DOI: 10.1021/acsomega.8b01071
ACS Omega 2018, 3, 9126−9145

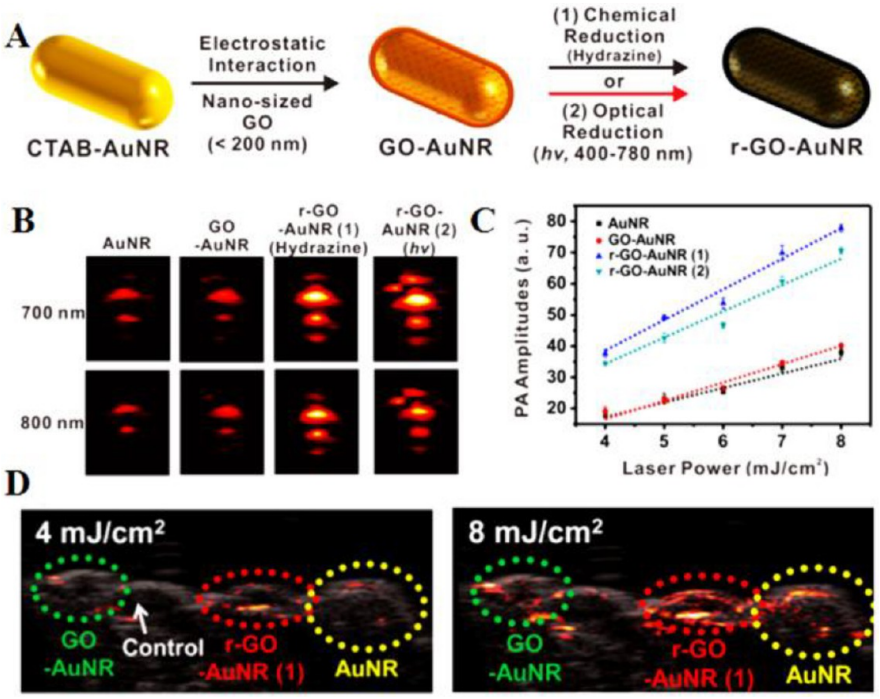

Figure 6. (A) Overall synthesis schemes of GO-AuNRs and rGO-AuNRs. (B) Representative PA images obtained using excitation wavelengths of 700 and 800 nm (input laser power, 6.2 mJ/cm^2; pulse rate, 10 Hz). (C) Photoacoustic amplitudes obtained with different laser power inputs. (D) Photoacoustic images of AuNRs, GO-AuNRs, and rGO-AuNRs in live mice. Overlaid ultrasound (gray) and photoacoustic (red) images. Reprinted with permission from ref 137. Copyright 2015 American Chemical Society.

2.1.4. Photoacoustic (PA) Imaging and Therapy. Photoacoustic (PA) imaging, serving as a biophotonic diagnostic modality, is mainly achieved by a safe thermal expansion mechanism.[129,130] A PA signal is generated within the compounds when they are irradiated by short-time laser pulses.[130] Although PA imaging overcomes the optical diffusion limit and gives access to deeper tissue imaging by combining optical excitation with ultrasonic detection, its sensitivity, determined by the compounds' light absorbance and heat capacity, is quite limited.[131−133] Thus, it is necessary to improve the conversion efficiency of light energy to thermal energy in order to achieve sensitive PA imaging. Recently, various PA contrast agents with remarkable optical absorbance properties, such as gold nanoparticles (AuNPs) and gold nanorods (AuNRs), have been widely employed in efforts to enhance PA imaging sensitivity.[134,135] It was demonstrated that the efficiency of heat transfer between heterogeneous materials played a significant role in obtaining amplified PA intensity.[136] Numerous studies have highlighted graphene-based heterogeneous systems as promising imaging agents for achieving high-resolution PA imaging. For example, Moon and co-workers produced rGO-coated AuNRs with superior amplified PA performance.[137] In this case, positively charged AuNRs were dropped onto the negatively charged rGO (Figure 6). The improved PA signal amplitude effect can reduce the damage to normal tissues from laser or imaging agents.

In another study, a new nanocomposite of indocyanine green-loaded polydopamine-rGO (ICG-PDA-rGO) was developed in order to simultaneously obtain an amplified PA signal and imaging-guided therapy effects.[138] The ICG-PDA-rGO showed not only prominent PA imaging sensitivity but also sufficient photothermal ablation effect for tumor. Overall, these studies provide remarkable evidence for the benefits of combining PA contrast agents with GO sheets to enhance PA intensity.

2.1.5. Radionuclide Imaging and Therapy. Radionuclide imaging (positron emission tomography (PET) and single-photon emission computed tomography (SPECT)), an imaging modality to measure biochemical metabolism, requires radiolabeled imaging agents (e.g., ^{64}Cu, ^{66}Ga, and ^{125}I).[139−141] Numerous molecules, such as antibodies,[142] nucleic acids,[143] small-molecule ligands,[144] and especially peptides,[145−147] have been labeled with radionuclides as PET probes.[148] Although decent tumor uptake was shown, fast clearance of the radiolabeled molecules from the tumors and short half-lives of the radionuclides limited their application in longitudinal tumor detection and radiation therapy (RT).[149,150]

Recently, some studies have been focused on the incorporation of radiolabeled molecules with GO for integration of imaging and therapeutic components. For example, Shi et al. designed ^{64}Cu-labeled and antibody-conjugated rGO for tumor vasculature-targeted PET imaging and PTT.[151] The resulting ^{64}Cu-NOTA-rGO-TRC105 exhibited long-term high aggregation in tumor and favorable PTT effect. In addition, Yang et al. similarly synthesized functionalized rGO with ^{64}Cu and antibody for PET early metastasis detection, targeted delivery of chemotherapeutics and PTT.[152] Moreover, Chen et al. developed ^{131}I-labeled rGO-PEG for SPECT imaging-guided RT and PTT for cancer.[153]

2.1.6. Multimodal Imaging and Therapy. Multimodal imaging has attracted increasing interest to overcome the limitations of single-modal imaging.[154−156] To achieve various modalities' integration, incorporation of independent modal contrast agents into a flexible platform has gradually become a main strategy.[157,158] However, this way usually requires complicated synthetic procedures and harsh conditions.

DOI: 10.1021/acsomega.8b01071
ACS Omega 2018, 3, 9126−9145

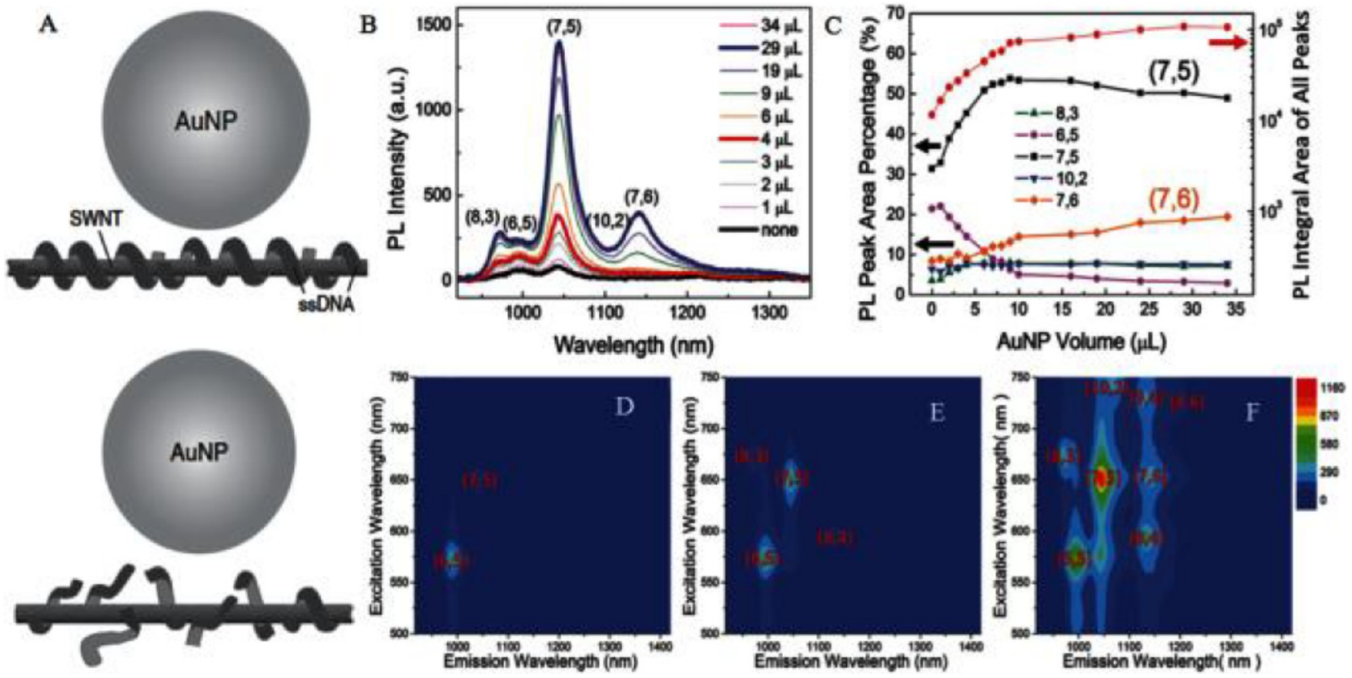

Figure 7. (A) Schematic of PL enhancement of the recognition DNA-SWNT pair and the non-recognition DNA-SWNT pair. (B) PL emission spectra upon excitation at 650 nm of AuNP-$(ATT)_4$AT-SWNTs with addition of concentrated AuNPs from 0 to 34 μL. (C) PL integral area of all peaks (red dots) and PL peak area percentage in (B). PLE maps of (D) the original $(ATT)_4$AT-SWNTs solution, (E) solution with addition of 4 μL of AuNPs, and (F) solution with addition of 29 μL of AuNPs. PL intensities for (D)−(F) follow the same color scale. Reprinted with permission from ref 29. Copyright 2016 Wiley-VCH Verlag GmbH & Co. KGaA.

Graphene is a competent platform due to its unique merits, such as large surface area, remarkable $\pi-\pi$ interactions, and electronic properties.[159,160] Xu et al. developed an integrated imaging system (^{64}Cu-rGO-IONP-PEG) combining MRI with PET and PA imaging to obtain higher quality imaging and more precise diagnostic data.[161] PET with high sensitivity and quantitative analysis, MRI featuring with high spatial resolution, and PA imaging giving access to deep tissue detection are excellent complements for disease diagnosis. In a follow-up report, photosensitizer was loaded onto nanographene via $\pi-\pi$ stacking for multimodal-imaging-guided synergistic therapy. The resulting GO-PEG-[^{64}Cu]HPPH achieved not only PET, PA, and fluorescence imaging simultaneously but also trimodal-guided tumor PDT.[162] In addition, Jin et al. developed poly(lactic acid) (PLA) microcapsules encapsulating GO and AuNPs for tumor PTT guided by ultrasound (US)/computed tomography (CT) bimodal imaging.[163] The PLA microcapsule can enhance US imaging. AuNPs with X-ray attenuation properties enable the use of CT contrast agents or radiosensitizers.[164−166] Meanwhile, AuNPs can enhance the effect of GO serving as a NIR-light absorbing agent, which efficiently converts absorbed light into heat. These studies give powerful evidence that graphene can serve as a multimodal imaging platform for tumor theranostic applications and can, to some extent, overcome the limitations of other platforms.

2.2. Single-Walled Carbon Nanotubes (SWNTs). *2.2.1. Fluorescence Imaging and Therapy.* The inherent chirality-characteristic PL of semiconducting SWNTs is characterized by NIR-I region excitation, large Stokes shift, ultralow autofluorescence background, and deep tissue penetration.[167−170] PL of SWNTs occurs when electron−hole (*e*-*h*) pairs recombine to emit a photon.[171,172] Some studies have been reported about PL of SWNTs in micelle solutions, air, and polymers.[173] However, the relatively low quantum yield (QY) of SWNTs (typically 0.1%−1.5%) severely restricted its further bioapplications.[174,175] It is well documented that the localized surface plasmon resonance (LSPR) of noble metals (e.g., gold or silver) enables surface-enhanced fluorescence (SEF).[176,177] The space between the carrier and the precious metal surface has a close relationship with SEF that is proportional to QY.[178−180] One of the key approaches to enhance the fluorescence as well as depress the quenching effect is to find a good linker that can closely connect noble metals to the surface of the SWNTs yet protect the SWNTs from direct conjugation. For this, Yang and co-workers attached DNA to the surface of SWNTs via $\pi-\pi$ stacking interactions and then assembled AuNPs onto the DNA-SWNTs, resulting in formation of AuNP-DNA-SWNT hybrids (Figure 7).[29] The DNA, serving as a spacer, separated AuNPs from SWNTs to achieve excellent SEF from the SWNTs. Compared with the SWNTs, the PL of AuNP-DNA-SWNTs was greatly more enhanced. In addition to the above method of locating noble metals on the SWNTs surface, PEGylated phospholipids were also used to enhance intrinsic PL and strengthen optical absorbance in the NIR.[181] The modified SWNTs were characterized by not only superior PL imaging but also a greater PTT effect compared to AuNRs. In a similar study, SWNTs were sonicated with sodium cholate, followed by surfactant DSPE-mPEG$_{5k}$ exchange, to form phospholipid−polyethylene glycol (PEG)-coated SWNTs (referred to as exchange-SWNTs) for NIR imaging.[182] The NIR PL of exchange-SWNTs is better than that of direct SWNT/DSPE-mPEG$_{5k}$ conjugates. Overall, despite the relatively low quantum yield (QY) of SWNTs, the functionalized SWNTs with inorganic materials (e.g., noble metal Au

DOI: 10.1021/acsomega.8b01071
ACS Omega 2018, 3, 9126−9145

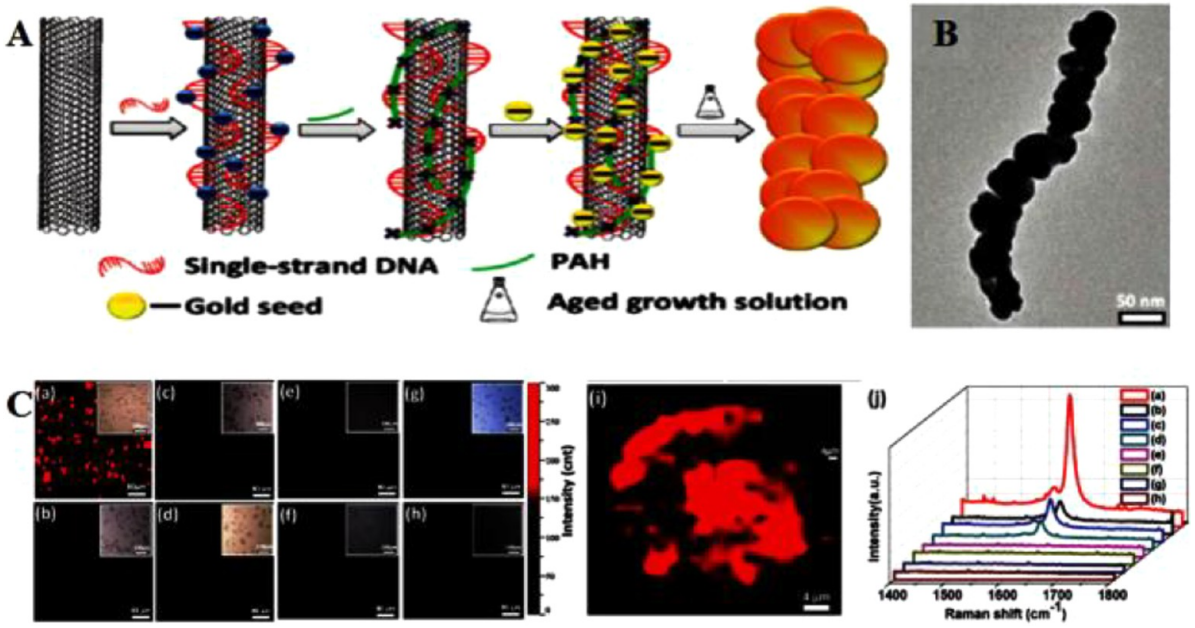

Figure 8. (A) Schematic illustration of the synthesis of SWNT−metal nanocomposites. (B) Representative TEM images of the SWNT-Au-PEG nanocomposite. (C) Raman imaging and averaged Raman spectra of cells. (a−h) Raman images of SWNT-Au-PEG-FA (a,b), SWNT-Au-PEG (c,d), SWNT-PEG-FA (e,f), and SWNT-PEG (g,h) labeled KB (a,c,e,g) and HeLa (b,d,f,h) cells. Reprinted with permission from ref 188. Copyright 2012 American Chemical Society.

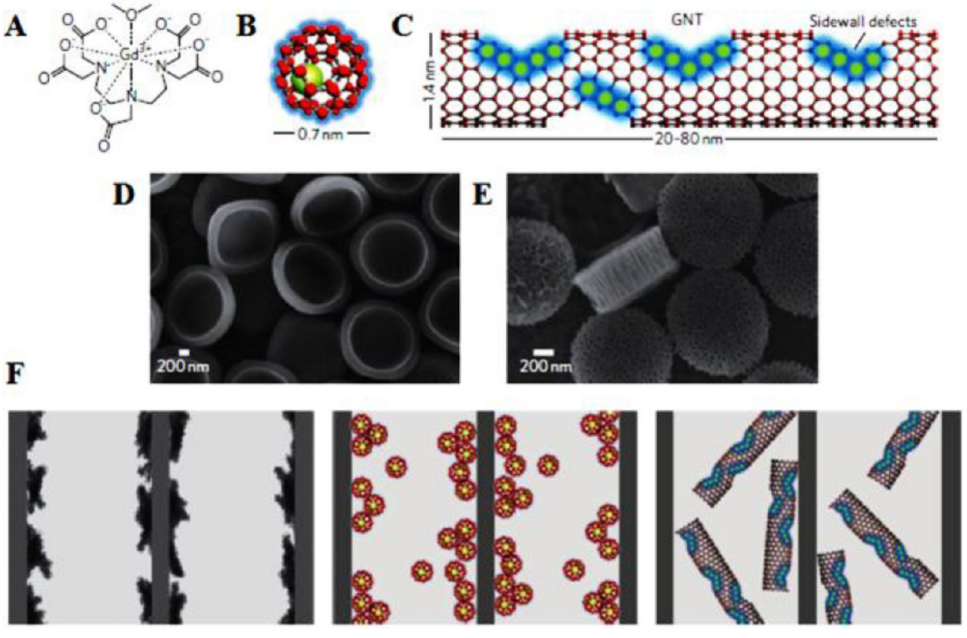

Figure 9. New MRI nanoconstructs. Schematic showing Magnevist (A), gadofullerenes (GFs) (B), and debundled gadonanotubes (GNTs) (C). Scanning electron micrographs of (D) quasi-hemispherical and (E) discoidal particles. (F) Cartoons showing Magnevist, GFs, and GNTs (left to right) entrapped within the porous structure of the SiMPs. Reprinted with permission from ref 193. Copyright 2010 Nature Publishing Group.

and Ag) or organic material (e.g., PEG and DNA) can show greatly enhanced PL and have superior prospects in NIR PL bioimaging.

2.2.2. Raman Imaging and Therapy. SWNTs with typical Raman spectra can give access to Raman imaging.[183] The characteristic structure of SWNTs can produce sharp van Hove singularities under the electronic density of states (eDOS), which results in the occurrence of resonant Raman scattering.[184] Compared with graphene, SWNTs themselves can produce stronger characteristic resonance-enhanced Raman peaks with tangential G bands (~1580 cm^{-1}) away from the excitation wavelength, which contributes to sensitive detection of unmodified SWNTs by Raman microspectroscopy.[113,185] Heller et al. first reported the intrinsic Raman properties of SWNTs for live cell imaging.[186] In their work, DNA-modified SWNTs (DNA-SWNTs) were used as cell markers that retained persistent Raman scattering in live cells, which allowed them to be used for long-term tracking in biological samples over months. Liu et al. investigated the biodistribution of functionalized SWNTs by invasive Raman

DOI: 10.1021/acsomega.8b01071
ACS Omega 2018, 3, 9126−9145

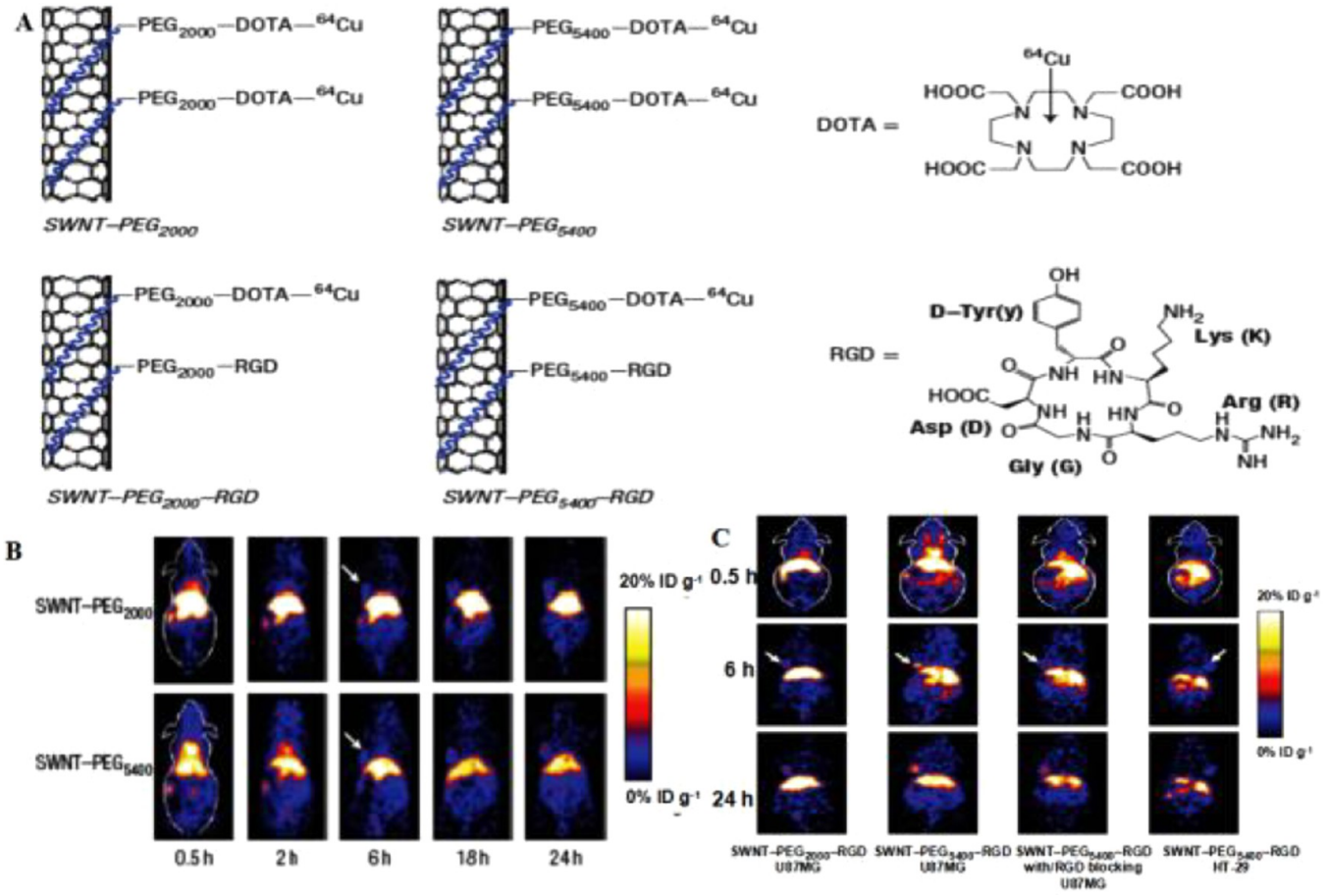

Figure 10. (A) Schematic drawings of non-covalently functionalized SWNT-PEG2000, SWNT-PEG5400, SWNT-PEG2000-RGD, and SWNT-PEG5400-RGD with DOTA-^{64}Cu. (B) MicroPET images of two mice at various time points post tail-vein injection of ^{64}Cu-labeled SWNT-PEG2000 and SWNT-PEG5400, respectively. (C) MicroPET images of mice. Reprinted with permission from ref 187. Copyright 2007 Nature Publishing Group.

spectroscopy of excised tissues to confirm the targeting effect.[187] Zavaleta et al. analyzed the targeting effect of arginine-glycine-aspartic acid (RGD) peptide-modified SWNTs by non-invasive Raman imaging in vivo.[28] Although SWNTs exhibit the appropriate inherent Raman signals, too much time is required to get a satisfactory Raman image.[183] It was hoped that SERS might overcome this obstacle. As such, Wang et al. developed a folic acid (FA)-conjugated SWNT-Au nanocomposite (SWNT-Au-PEG-FA) for PTT and SERS imaging whose imaging time was remarkably shortened compared to that of targeted SWNTs (Figure 8).[188]

2.2.3. Magnetic Resonance Imaging and Therapy. In addition to graphene, SWNT-based nanomaterials were also used as scaffolds to anchor MNPs or Gd^{3+}-based agents in order to improve the imaging quality. MNPs/Gd^{3+} clustering on SWNTs sheets would not only enhance MRI contrast but also improve the physiological stability of the aggregated MNPs/Gd^{3+}.[189,190] To this end, Sitharaman et al. developed ultra-short SWNTs (US-tubes) with nanoscale loading and confinement of $Gd^{3+}{}_n$ clusters to enhance longitudinal relaxivity, r_1.[191] The MRI efficacies of these $Gd^{3+}{}_n$@US-tubes were 40−90 times larger than those of clinical used Gd^{3+}-based contrast agents. Safety development of Gd^{3+}n@US-tube as contrast agents was later demonstrated by Holt et al.[192] Further advancing upon these hybrid platforms, Gd^{3+}-SWNTs were confined inside the nanoporous structure of silicon particles (SiMPs) by Ananta et al. to improve nanoscale confinement for enhancement of the image contrast.[193] The r_1 relaxivity of the resulting SiMPs/Gd-SWNTs composites increased by approximately 1.5 times compared to that of Gd-SWNTs (Figure 9). The enhancement in contrast can be attributed to the geometrical confinement of the agents, which largely increased their tumbling time (τ_R). Therefore, nanoscale confinement could serve as a new and general strategy to enhance the contrast of MNPs or Gd^{3+}-based contrast agents.

Recently, to integrate imaging and therapy function, Hou et al. developed a targeted multifunctional theranostic system based on Gd^{3+}-SWNTs. Herein, hyaluronic acid (HA)-modified SWNTs (SWNTs-HA) were first synthesized, and then DOX was conjugated with HA by disulfide bonds (SWNTs-HA-ss-DOX). Finally, Gd^{3+} ions were loaded on the sidewall defects of SWNTs.[37] When Gd/SWNTs-HA-ss-DOX were uptaken into cancer cells, high concentrations of glutathione (GSH) broke the disulfide bond, which resulted in DOX release to achieve precise chemotherapy.

In addition to the above studies, mainly referring to T_1-weighted images, T_2 negative contrast agents based on MNPs-SWNTs have also been widely studied.[36] Recently, Al Faraj et al. employed an iron-tagging method to successfully develop iron-tagged and antibody-conjugated SWNTs for enhanced magnetic targeting and non-invasive MRI monitoring.[194] Therefore, perhaps Gd-based T_1 or MNPs-based T_2 contrast

DOI: 10.1021/acsomega.8b01071
ACS Omega 2018, 3, 9126−9145

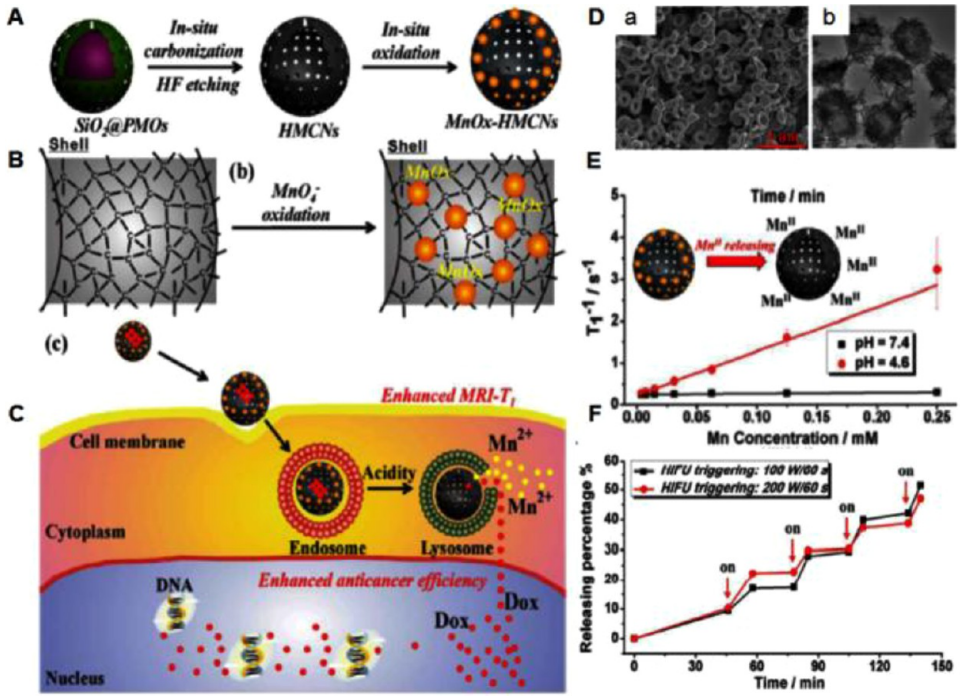

Figure 11. Schematic illustration of (A) synthetic procedure for MnOx-HMCNs, (B) incorporation of MnOx NPs into the framework of HMCNs, and (C) cellular uptake and dual pH-responsiveness of MnOx-HMCNs for T_1-weighted MRI and anti-cancer drug release. (D) (a) SEM image of RBCs-shaped HMCNs and (b) TEM images of MnOx-HMCNs with low magnification. (E) Plot of T_1^{-1} versus Mn concentration of MnOx-HMCNs. (F) HIFU-triggered DOX release percentage under different irradiation parameters. Reprinted from ref 49 with permission from The Royal Society of Chemistry.

agents conjugated with SWNTs could reach great imaging effects even for better imaging and treatment.

2.2.4. Radionuclide Imaging and Therapy. Similar to graphene, radiolabeled SWNTs conjugates also have been explored. Liu et al. reported ^{64}Cu-radiolabeled SWNTs functionalized with phospholipid-PEG (PL-PEG$_{5400}$) and RGD peptide (Figure 10).[187] PEGylation imparted to SWNTs high hydrophilicity and resistance to protein non-specific binding, which resulted in reduced RES uptake, long blood circulation, and stable PET imaging of ^{64}Cu-labeled SWNT-PEG-RGD. In addition, Cisneros and co-workers successfully loaded $^{64}Cu^{2+}$ ions into SWNTs platform by sonication without the use of chelating ligands.[195] The new strategy achieved stable loading of contrast agents. The resulting ^{64}Cu@GNTs give access to excellent imaging quality.

2.2.5. Multimodal Imaging and Therapy. To sum up, semiconducting SWNTs, characterized by remarkable resonance-enhanced Raman scattering, alluring PL, and strong optical absorption in the NIR region, could be competent multimodal imaging platforms. Given this, Wang et al. designed targeted SWNTs with attached Fe/Co nanoparticles to label human mesenchymal stem cells (hMSCs).[196] The multimodal imaging platform gives access to triple-modal imaging, including strong Raman signals, T_2-weighted MR images, and intense PA signals. These functionalized SWNTs were characterized by high chemical stabilities and photostabilities. This study highlighted the potential of well-functionalized SWNTs as multimodal imaging probes. For further therapy under multimodal imaging guidance, Zhao et al. prepared Mn^{2+}-chelated and ^{31}I-radiolabeled SWNTs as a theranostic platform for tumor multimodal imaging and therapy.[197] Their previous work confirmed that PDA with phenol groups could be efficiently labeled with radioactive iodine (e.g., ^{131}I) using the chloramine-T oxidation method. PDA-modified SWNTs were labeled with ^{131}I using the same method used for tumor gamma imaging. Depending on the inherent strong NIR absorbance of SWNTs, ^{131}I-based radioactivity and T_1/T_2 MRI of Mn^{2+}, the functionalized SWNTs achieved magnetic resonance and gamma bimodal imaging-guided PTT and radioisotope therapy under NIR.

2.3. Imaging and Therapy-Based Mesoporous Carbon. Three-dimensional MCNs with high drug loading and controlled drug release capability are highly desirable to establish an intelligent stimuli-responsive cancer theranostic system which can reduce adverse effects of cytotoxic drugs and achieve treatment monitoring.[198] Recently, MCNs combining both imaging contrast agents and drugs simultaneously have received much attention. Zhou et al. reported DOX-loaded colloidal mesoporous carbon nanospheres (Meso-CNs) for tumor PTT and PA imaging.[199] By side-by-side comparisons with SWNTs, graphene, and AuNRs, the Meso-CNs were shown to possess higher absorption coefficients than those of CNTs and graphene, and even comparable with those of AuNRs. Moreover, Zhang et al. synthesized DOX-loaded hollow mesoporous silicon/carbon (Si/C) NPs (PEG-Si/C-DOX) for highly effective PA imaging-guided chemo-thermal tumor therapy.[200] Zhang et al. constructed a highly efficient multiple-stimuli-responsive nanosystems based on hollow MCNs (HMCNs) for pH-responsive MRI and on-demand drug release (Figure 11).[39] Manganese oxide (MnOx) NPs can be *in situ* generated and incorporated into the framework or onto the surface of HMCNs to form MnOx-HMCNs by a redox reaction between $KMnO_4$ and a carbonaceous framework of HMCNs. The "OFF" state that kept Mn atoms restricted within the MnOx NPs can been broken up by the acidic microenvironment in tumor cells to release Mn^{2+} ions,

DOI: 10.1021/acsomega.8b01071
ACS Omega 2018, 3, 9126−9145

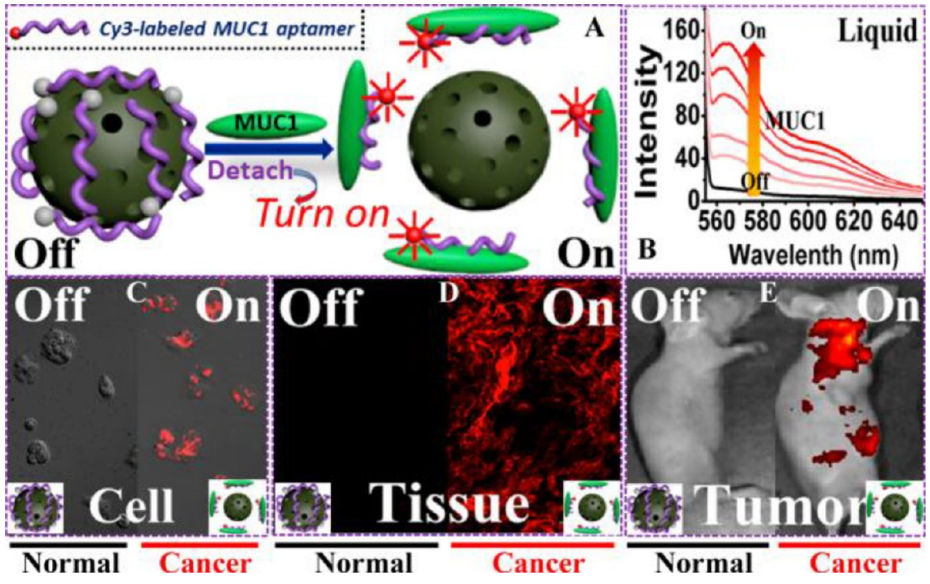

Figure 12. (A) Schematic illustration of the sensing principle based on the OMCN/P_0-Cy3 aptasensor. (B) MUC1-responsive fluorescence recovery in the buffer solution recorded by fluorescence spectrophotometry. (C−E) Sensing performance of the OMCN/P0-Cy3 aptasensor at cell level (confocal fluorescence microscopy image), tissue level (inverted fluorescence microscopy image), and whole animal level (in vivo fluorescent image), respectively. Reprinted with permission from ref 49. Copyright 2015 American Chemical Society.

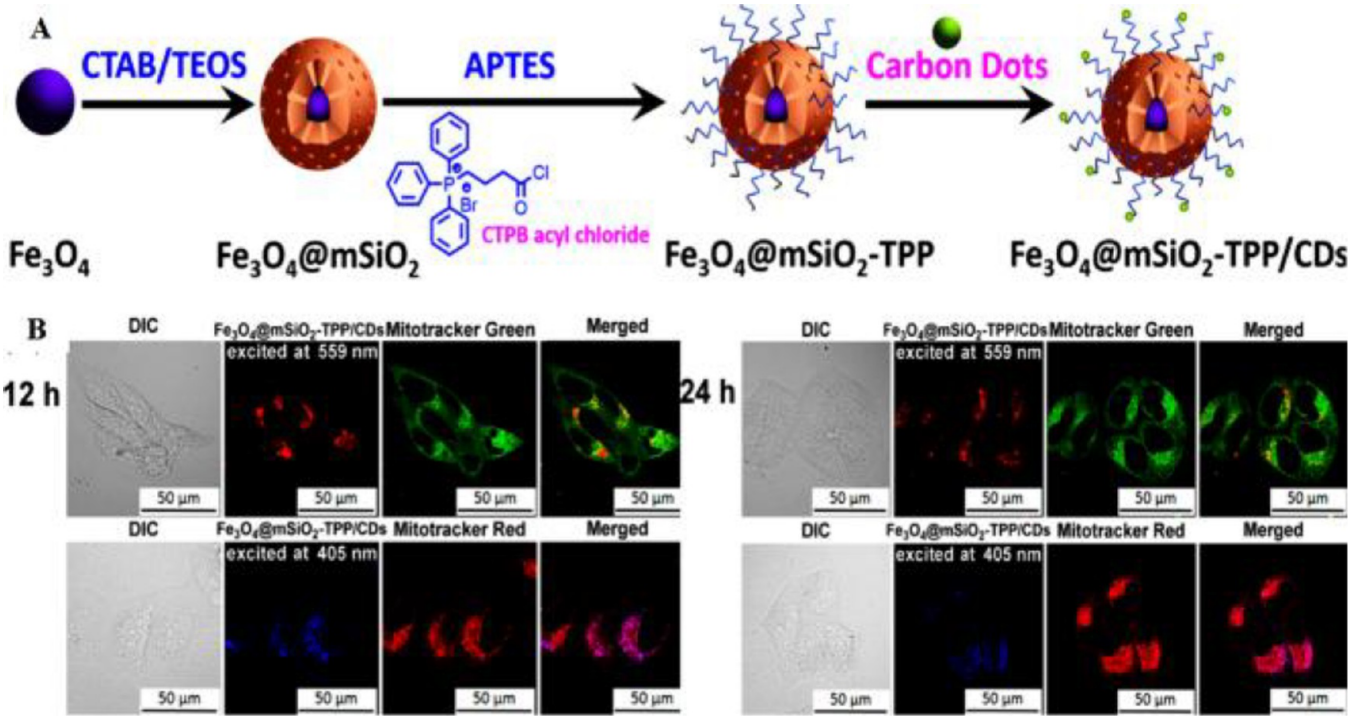

Figure 13. (A) Schematic route for the synthesis of Fe_3O_4@$mSiO_2$-TPP-CDs nanoplatform. (B) Differential interference contrast and confocal laser scanning microscopy images of HeLa cells exposed to 100 μg/mL of Fe_3O_4@$mSiO_2$-TPP/CDs. Reprinted with permission from ref 210. Copyright 2015 American Chemical Society.

which result in significantly enhanced T_1 performance ("ON" state). Importantly, DOX loaded onto MnOx-HMCNs through $\pi-\pi$ stacking was also highly sensitive to pH variations. In addition, introduction of high-intensity focused ultrasound could significantly accelerate the release rate of DOX from MnOx-HMCNs.

Furthermore, a GQDs-based fluorescent mesoporous carbon nanoshell (FMP-CNS) was developed as a hydrophobic drug carrier that integrated functions of stimuli-responsive drug release, multimodal optical imaging, and photothermal therapy/chemotherapy.[48] The FMP-CNS can serve as an optical marker for confocal, two-photon, and NIR fluorescence imaging. Moreover, the hydrophobic drug paclitaxel (PTX), loaded on the FMP-CNS, can be controllably released under NIR irradiation. MCNs can also carry fluorescent dyes. In a recent study, a fluorescent probe based on oxidized MCNs (OMCNs)was constructed, wherein Cy3-labeled ssDNA (P_0 aptamer) was loaded on the surface of OMCNs by $\pi-\pi$

DOI: 10.1021/acsomega.8b01071
ACS Omega 2018, 3, 9126−9145

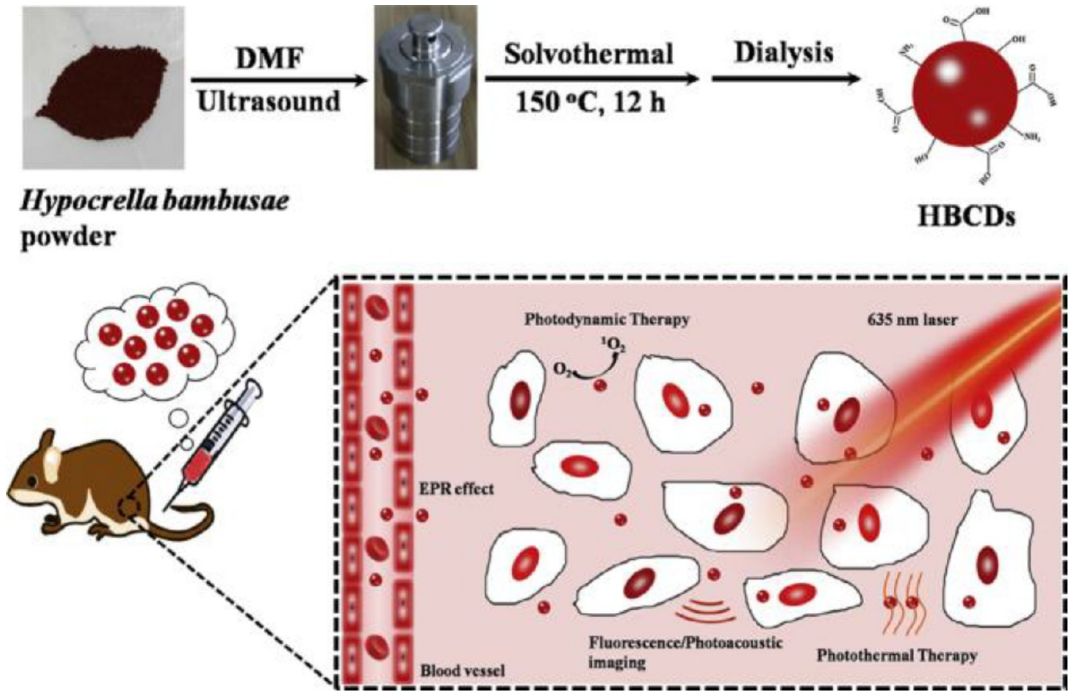

Figure 14. Schematic of synthesis of HBCDs derived from *Hypocrella bambusae* for tumor bimodal FL/PA imaging-guided synergistic PDT/PTT. Reprinted with permission from ref 214. Copyright 2018 Elsevier B.V.

stacking, resulting in almost complete fluorescence quenching (Figure 12).[49] The P_0 aptamer can specifically bind to the cell-surface mucin1 (MUC1) marker which is overexpressed in many malignant tumors (e.g., breast cancer and prostate cancer). Once exposed to MUC1, P_0 aptamer, separated from OMCN, decomposed to achieve fluorescence recovery.

2.4. Imaging and Therapy-Based Carbon Dots. At present, CDs are receiving considerable attention for potential theranostic applications owing to their unique superior properties, such as inherent favorable aqueous solubility, good photostability, easy modification, low toxicity, and excellent biocompatibility.[201−206] For example, Cao et al. demonstrated the potential of CDs for cell imaging with two-photon excitation in the NIR.[59] Later, Yang et al. reported the first use of CDs for optical imaging in vivo.[207] Recently, a new type of fluorescent carbon dots (CD-Asp), with the ability to specifically target glioma, were successfully synthesized via a simple thermolysis route using D-glucose and L-aspartic acid as starting materials.[208] CD-Asp could act as a targeting fluorescence imaging agent for non-invasive glioma diagnosis, and has the potential for use in constructing an intelligent nanomedicine integrating diagnostic, targeting, and therapeutic functions. In addition, there have also been some studies about the use of functionalized CDs for multimodal imaging. Zhang et al. employed a hydrothermal carbonization (HTC) approach for facile preparation of iodine-doped carbon dots (I-doped CDs).[209] The resulting CD composites exhibited not only favorable PL but also high X-ray attenuation. In another study, targeted magnetic mesoporous silica nanoparticles (Fe_3O_4@mSiO_2) with fluorescent CDs were constructed for fluorescence imaging and MRI (Figure 13).[210]

However, the complex synthetic route and high cost of CDs greatly limit their practical applications. To address this issue, a highly promising approach for the synthesis of carbon materials is based on the use of well-defined molecular precursors.[211] Ge et al. prepared novel CDs using poly-thiophene phenylpropionic acid (PPA) as the precursor for fluorescence/PA imaging-guided cancer PTT.[212] Li et al. successfully synthesized tetraphenylporphyrin-based carbon dots (TPP CDs) for PDT of hepatoma.[213] The TPP CDs can efficiently generate $^1O_2$, resulting in significant cancer PDT efficacy. Jia et al. employed *Hypocrella bambusae* (HB) as a raw carbon source to successfully synthesize *H. bambusae* CDs (HBCDs) which could be served as theranostic agents for bimodal fluorescence/PA imaging-guided cancer synergistic PDT/PTT (Figure14).[214] The obtained HBCDs showed good water solubility, broad absorption, red-light emission, and excellent biocompatibility. Similarly, another type of CDs with intrinsic theranostic properties were prepared by using polythiophenebenzoic acid (PBA) as carbon source for imaging-guided PDT/PTT.[215] The novel CDs from PBA exhibited properties similar to those of the above HBCDs. Jia et al. designed multifunctionalized CDs on the surface of SiO_2-coated AuNRs (AuNR@SiO_2-CDs) as phototheranostics for cancer PDT/PTT synergistic therapy under the guidance of FL and PA imaging.[54]

2.5. Imaging and Therapy-Based Other Carbon Nanomaterials. Nanodiamonds (NDs) can emit significant fluorescence and present perfect photostability with no photobleaching, making them useful for bioimaging without further functionalization.[72,216] Massive research efforts have been devoted to the utilization of NDs as fluorescent markers for cellular tracking in vivo/in vitro.[69,72,217] In addition, NDs are characterized by facet-specific electrostatic properties which contribute to coordination of water molecules on specific facets. Thus, NDs themselves, to an extent, improve the effect of MRI contrast agents. In one study, Hou et al. conjugated Gd to a NDs surface to acquire T_1/T_2 dual-mode MR imaging.[218] Furthermore, Waddington et al. demonstrated that the nuclear Overhauser effect, a proton−electron polarization transfer technique, enables high-contrast MRI of unfunctionalized NDs in water.[219] The technique significantly

DOI: 10.1021/acsomega.8b01071
ACS Omega 2018, 3, 9126−9145

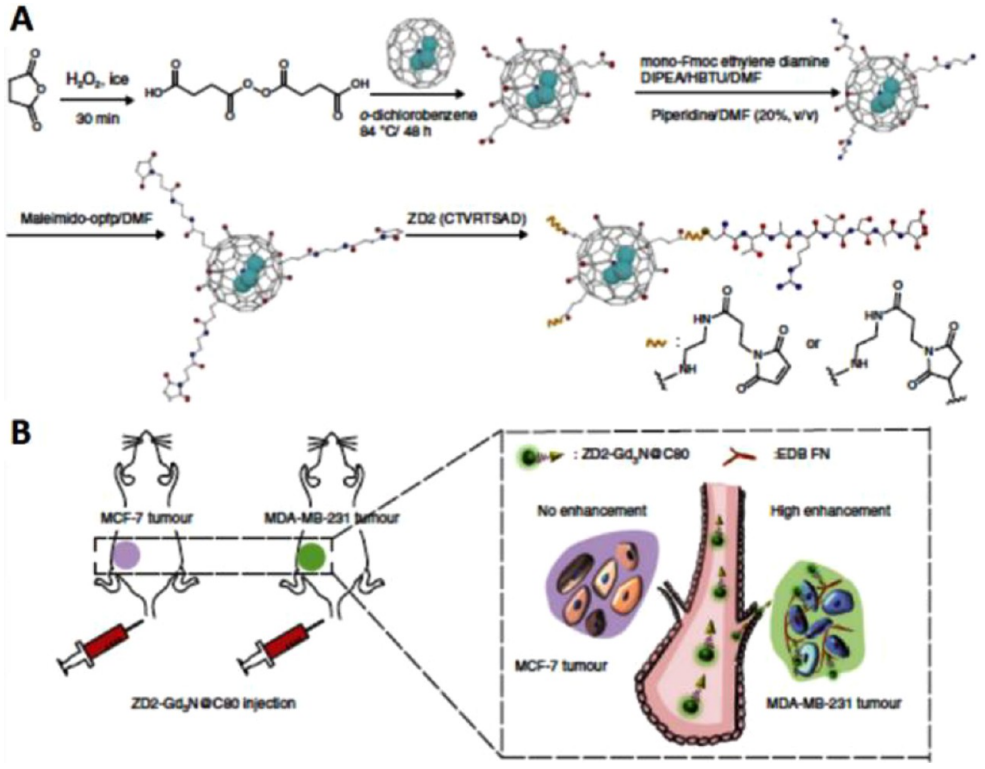

Figure 15. (A) Schematic illustration of ZD2-$Gd_3N@C_{80}$ probes. (B) Illustration of tumor targeting with the probes for detection of breast cancer. Reprinted with permission from ref 226. Copyright 2017 Nature Publishing Group, http://creativecommons.org/licenses/by/4.0/).

expanded the theranostic capabilities of NDs and opened the possibility that NDs themselves can serve as MR contrast agents. Recent in vivo studies reported the clinical potential of utilizing NDs to deliver chemotherapeutic agents.

Due to their surface-dependent PL, excellent photostability, and biocompatibility, fullerenes can be used for fluorescence imaging.[220] For example, hyaluronated C_{60} fullerene with a strong intrinsic NIR fluorescence emission was designed for both fluorescence imaging and PDT of HCT-116 tumors (CD44+).[221] In addition, Tan and co-workers presented a photoluminescent fullerene-capped MSN system for bioimaging and pH-responsive drug delivery.[222] Recently, metallofullerenes containing Gd complexes (e.g., Gd@C_{60}, Gd@C_{82}, and $Gd_3N@C_{80}$) have been employed as MR contrast agents with much higher relaxivity and safety than most commercial Gd-chelator agents.[223−225] Gd-ion-associated toxicity is decreased by confining Gd ions inside a robust carbon cage to suppress their leakage. Therefore, the development of Gd-containing metallofullerene contrast agents is highly desirable for multimodal imaging. Han et al. synthesized a high-relaxivity-targeted $Gd_3N@C_{80}$ contrast agent (ZD2-$Gd_3N@C_{80}$) by conjugating a small targeting peptide, ZD2 (Cys-Thr-Val-Arg-Thr-Ser-Ala-Asp), for sensitive molecular MRI of breast cancer (Figure 15).[226] Wang et al. developed radionuclide ^{64}Cu-labeled DOX-loaded PDA-gadolinium-metallofullerene ($Gd_3N@C_{80}$, denoted as CDPGM) core−satellite nanotheranostics for multimodal imaging-guided combination cancer therapy.[227] Besides T_1 MRI contrast agents, iron oxide (Fe_3O_4) nanoparticles and upconversion nanophosphors were also loaded onto C_{60} to achieve effective therapy and live surveillance of tumors.[228] Later, FA-modified C_{60}-IONP-PEG was designed to achieve targeted PDT, release and thermal therapy (RTT), and T_2 MRI.[101] Moreover, FA-modified C_{60}@Au hybrid aggregates were synthesized for radiofrequency-based controlled RTT, PDT synergetic therapy, and X-ray imaging.[229]

3. CHALLENGES AND FUTURE PROSPECTIVE

CBNs, as new stars in nanoresearch, have attracted increasing attention in the past few years in a wide array of fields, especially for biological applications such as bioimaging, drug delivery, and cancer therapeutics. In this article, we look at various applications of MCBNs in tumor molecular bioimaging and imaging-guided molecular-level cancer therapy. As a primary conclusion based on the considerable research over the past two decades, it can be said that MCBNs have tremendous potential in early comprehensive diagnosis and precise treatment of cancer due to their intrinsic physicochemical properties.

Although molecular imaging has demonstrated promising potential for MCBNs and will play a significant role pertaining to increased theranostic accuracy as well as improved prognosis of disease, the most realistic direction for highly sensitive and non-invasive theranostic technology is its application to patient care. This means that there are considerable challenges to be addressed before MCBNs can be translated into actual use in clinical practice. Although various functionalization strategies have been developed to reduce toxicity and improve biocompatibility, efforts are still needed to further implement more systematic toxicology studies to determine the interactions between MCBNs and physiological systems and the pharmacokinetics of MCBNs according to U.S. FDA guidelines.

In order to reduce undesirable side effects on the human body, "precision medicine", which involves accurate localization and precise removal of tumors under imaging guidance,

DOI: 10.1021/acsomega.8b01071
ACS Omega 2018, 3, 9126−9145

has become the current cutting-edge topic. Some researches have made use of tumor's microenvironment to active targeting, based on, e.g., low pH, high H_2O_2, and abundant GSH. On the other hand, by controlling the size of the nanomaterials in order to avoid liver and spleen phagocytosis, some researches have optimized the permeability and retention effects of MCBNs to notably improve passive targeting. Although these are exciting strategies, a significant concern that remains is how to precisely target tumor sites to achieve accurate diagnoses and therapy.

For cancer theranostics, image-guided synergistic therapy and intelligent drug delivery systems are the most promising trends. In order to acquire more comprehensive disease information, which is essential for diagnosis and treatment, multimodal imaging is practically feasible for overcoming the inherent limitations of each modality alone. MCBNs can serve as a multiplatform, gathering different imaging agents and therapeutic drugs for cancer diagnosis and therapy integration. Despite the certain challenges and unresolved obstacles, MCBNs have potential clinical advantages as imaging and treatment agents and will be more likely to be applied in clinical settings in the near future. Finally, significant investigation will be required to further develop advanced carbonaceous nanomaterials for improving the efficacy of theranostics and reduce side effects. Once MCBNs are established in that field, their applications in theranostics would become more realistic.

AUTHOR INFORMATION

Corresponding Author

*Tel.: 022-88329407. E-mail: luckyxn_tianjin@163.com.

ORCID

Yanyan Zhang: 0000-0001-5975-7778

Author Contributions

#Yanyan Zhang, Minghao Wu, and Mingjie Wu contributed equally to this work.

Notes

The authors declare no competing financial interest.

ACKNOWLEDGMENTS

This work was financially supported by a project of the Key Program of the Tianjin Health and Family Planning Commission (16KG115), by the Tianjin Medical University "13th five-year" comprehensive investment subject construction project (116015012017XK0202), and by the Natural Science Foundation for Colleges and Universities in Jiangsu Province (17KJB350005). All the financial support is gratefully acknowledged.

REFERENCES

(1) Weissleder, R.; Pittet, M. J. Imaging in the era of molecular oncology. *Nature* **2008**, *452*, 580−589.

(2) Dou, Y.; Li, X.; Yang, W.; Guo, Y.; Wu, M.; Liu, Y.; Li, X.; Zhang, X.; Chang, J. PB@Au Core-Satellite Multifunctional Nanotheranostics for Magnetic Resonance and Computed Tomography Imaging in Vivo and Synergetic Photothermal and Radiosensitive Therapy. *ACS Appl. Mater. Interfaces* **2017**, *9*, 1263−1272.

(3) Narayanan, T. N.; Gupta, B. K.; Vithayathil, S. A.; Aburto, R. R.; Mani, S. A.; Taha-Tijerina, J.; Xie, B.; Kaipparettu, B. A.; Torti, S. V.; Ajayan, P. M. Hybrid 2D nanomaterials as dual-mode contrast agents in cellular imaging. *Adv. Mater.* **2012**, *24*, 2992−2998.

(4) Peng, Y.-K.; Lui, C. N. P.; Chen, Y.-W.; Chou, S.-W.; Raine, E.; Chou, P.-T.; Yung, K. K. L.; Tsang, S. C. E. Engineering of Single Magnetic Particle Carrier for Living Brain Cell Imaging: A Tunable T1-/T2-/Dual-Modal Contrast Agent for Magnetic Resonance Imaging Application. *Chem. Mater.* **2017**, *29*, 4411−4417.

(5) Chen, Y. W.; Liu, T. Y.; Chen, P. J.; Chang, P. H.; Chen, S. Y. A High-Sensitivity and Low-Power Theranostic Nanosystem for Cell SERS Imaging and Selectively Photothermal Therapy Using Anti-EGFR-Conjugated Reduced Graphene Oxide/Mesoporous Silica/AuNPs Nanosheets. *Small* **2016**, *12*, 1458−1468.

(6) Chen, D.; Dougherty, C. A.; Zhu, K.; Hong, H. Theranostic applications of carbon nanomaterials in cancer: Focus on imaging and cargo delivery. *J. Controlled Release* **2015**, *210*, 230−245.

(7) Goenka, S.; Sant, V.; Sant, S. Graphene-based nanomaterials for drug delivery and tissue engineering. *J. Controlled Release* **2014**, *173*, 75−88.

(8) Brakmane, G.; Madani, S. Y.; Seifalian, A. Cancer Antibody Enhanced Real Time Imaging Cell Probes-a Novel Theranostic Tool using Polymer Linked Carbon Nanotubes and Quantum Dots. *Anti-Cancer Agents Med. Chem.* **2013**, *13*, 821−832.

(9) Cha, C.; Shin, S. R.; Annabi, N.; Dokmeci, M. R.; Khademhosseini, A. Carbon-Based Nanomaterials Multifunctional Materials for Biomedical Engineering. *ACS Nano* **2013**, *7*, 2891−2897.

(10) Krüger, A. *Carbon Materials and Nanotechnology*; Wiley VCH Verlag GmbH: Weinheim, 2010; pp 475−475.

(11) Georgakilas, V.; Otyepka, M.; Bourlinos, A. B.; Chandra, V.; Kim, N.; Kemp, K. C.; Hobza, P.; Zboril, R.; Kim, K. S. Functionalization of graphene: covalent and non-covalent approaches, derivatives and applications. *Chem. Rev.* **2012**, *112*, 6156−6214.

(12) Novoselov, K. S.; Fal'ko, V. I.; Colombo, L.; Gellert, P. R.; Schwab, M. G.; Kim, K. A roadmap for graphene. *Nature* **2012**, *490*, 192−200.

(13) Bonaccorso, F.; Sun, Z.; Hasan, T.; Ferrari, A. C. Graphene photonics and optoelectronics. *Nat. Photonics* **2010**, *4*, 611−622.

(14) Stoller, M. D.; Park, S.; Zhu, Y.; An, J.; Ruoff, R. S. Graphene-based ultracapacitors. *Nano Lett.* **2008**, *8*, 3498−3502.

(15) Balandin, A. A.; Ghosh, S.; Bao, W.; Calizo, I.; Teweldebrhan, D.; Miao, F.; Lau, C. N. Superior thermal conductivity of single-layer graphene. *Nano Lett.* **2008**, *8*, 902−907.

(16) Sanchez, V. C.; Jachak, A.; Hurt, R. H.; Kane, A. B. Biological Interactions of Graphene-Family Nanomaterials − An Interdisciplinary Review. *Chem. Res. Toxicol.* **2012**, *25*, 15−34.

(17) Robinson, J. T.; Tabakman, S. M.; Liang, Y.; Wang, H.; Casalongue, H. S.; Vinh, D.; Dai, H. Ultrasmall reduced graphene oxide with high near-infrared absorbance for photothermal therapy. *J. Am. Chem. Soc.* **2011**, *133*, 6825−6831.

(18) Marcano, D. C.; Kosynkin, D. V.; Berlin, J. M.; Sinitskii, A.; Sun, Z.; Slesarev, A.; Alemany, L. B.; Lu, W.; Tour, J. M. Improved synthesis of graphene oxide. *ACS Nano* **2010**, *4*, 4806−4814.

(19) Kim, J.; Cote, L. J.; Kim, F.; Yuan, W.; Shull, K. R.; Huang, J. Graphene oxide sheets at interfaces. *J. Am. Chem. Soc.* **2010**, *132*, 8180−8186.

(20) Longchamp, J. N.; Latychevskaia, T.; Escher, C.; Fink, H.-W. Graphene Unit Cell Imaging by Holographic Coherent Diffraction. *Phys. Rev. Lett.* **2013**, *110*, 255501.

(21) Zhang, L.; Xia, J.; Zhao, Q.; Liu, L.; Zhang, Z. Functional Graphene Oxide as a Nanocarrier for Controlled Loading and Targeted Delivery of Mixed Anticancer Drugs. *Small* **2010**, *6*, 537−544.

(22) Kim, J.; Kim, F.; Huang, J. Seeing graphene-based sheets. *Mater. Today* **2010**, *13*, 28−38.

(23) Acik, M.; Lee, G.; Mattevi, C.; Chhowalla, M.; Cho, K.; Chabal, Y. J. Unusual infrared-absorption mechanism in thermally reduced graphene oxide. *Nat. Mater.* **2010**, *9*, 840−845.

(24) Li, D.; Muller, M. B.; Gilje, S.; Kaner, R. B.; Wallace, G. G. Processable aqueous dispersions of graphene nanosheets. *Nat. Nanotechnol.* **2008**, *3*, 101−105.

(25) Iijima, S. Helical microtubules of graphitic carbon. *Nature* **1991**, *354*, 56−58.

DOI: 10.1021/acsomega.8b01071
ACS Omega 2018, 3, 9126−9145

(26) Harrison, B. S.; Atala, A. Carbon nanotube applications for tissue engineering. *Biomaterials* **2007**, *28*, 344−353.
(27) Kyotani, T. Control of pore structure in carbon. *Carbon* **2000**, *38*, 269−286.
(28) Zavaleta, C.; de la Zerda, A.; Liu, Z.; Keren, S.; Cheng, Z.; Schipper, M.; Chen, X.; Dai, H.; Gambhir, S. S. Noninvasive Raman Spectroscopy in Living Mice for Evaluation of Tumor Targeting with Carbon Nanotubes. *Nano Lett.* **2008**, *8*, 2800−2805.
(29) Yang, J.; Zhao, Q.; Lyu, M.; Zhang, Z.; Wang, X.; Wang, M.; Gao, Z.; Li, Y. Chirality-Selective Photoluminescence Enhancement of ssDNA-Wrapped Single-Walled Carbon Nanotubes Modified with Gold Nanoparticles. *Small* **2016**, *12*, 3164−3171.
(30) Bachilo, S. M. Structure-Assigned Optical Spectra of Single-Walled Carbon Nanotubes. *Science* **2002**, *298*, 2361−2366.
(31) Kam, N. W. S.; Jan, E.; Kotov, N. A. Electrical Stimulation of Neural Stem Cells Mediated by Humanized Carbon Nanotube Composite Made with Extracellular Matrix Protein. *Nano Lett.* **2009**, *9*, 273−278.
(32) Liu, Z.; Yang, K.; Lee, S. T. Single-walled carbon nanotubes in biomedical imaging. *J. Mater. Chem.* **2011**, *21*, 586−598.
(33) Welsher, K.; Liu, Z.; Sherlock, S. P.; Robinson, J. T.; Chen, Z.; Daranciang, D.; Dai, H. A route to brightly fluorescent carbon nanotubes for near-infrared imaging in mice. *Nat. Nanotechnol.* **2009**, *4*, 773−780.
(34) Liu, Z.; Tabakman, S. M.; Welsher, K.; Dai, H. Carbon nanotubes in biology and medicine: In vitro and in vivo detection, imaging and drug delivery. *Nano Res.* **2009**, *2*, 85−120.
(35) Hong, G.; Diao, S.; Chang, J.; Antaris, A. L.; Chen, C.; Zhang, B.; Zhao, S.; Atochin, D. N.; Huang, P. L.; Andreasson, K.; Kuo, C. J.; Dai, H. Through-skull fluorescence imaging of the brain in a new near-infrared window. *Nat. Photonics* **2014**, *8*, 723−730.
(36) Choi, J. H.; Nguyen, F. T.; Barone, P. W.; Heller, D. A.; Moll, A. E.; Patel, D.; Boppart, S. A.; Strano, M. S. Multimodal Biomedical Imaging with Asymmetric Single -Walled Carbon Nanotube/Iron Oxide Nanoparticle Complexes. *Nano Lett.* **2007**, *7*, 861−867.
(37) Hou, L.; Yang, X.; Ren, J.; Wang, Y.; Zhang, H.; Feng, Q.; Shi, Y.; Shan, X.; Yuan, Y.; Zhang, Z. A novel redox-sensitive system based on single-walled carbon nanotubes for chemo-photothermal therapy and magnetic resonance imaging. *Int. J. Nanomed.* **2016**, *11*, 607−624.
(38) Wang, L.; Shi, J.; Jia, X.; Liu, R.; Wang, H.; Wang, Z.; Li, L.; Zhang, J.; Zhang, C.; Zhang, Z. NIR-/pH-Responsive drug delivery of functionalized single-walled carbon nanotubes for potential application in cancer chemo-photothermal therapy. *Pharm. Res.* **2013**, *30*, 2757−2771.
(39) Zhang, S.; Qian, X.; Zhang, L.; Peng, W.; Chen, Y. Composition-Property Relationships in Multifunctional Hollow Mesoporous Carbon Nanosystems for pH-Responsive Magnetic Resonance Imaging and On-Demand Drug Releasing. *Nanoscale* **2015**, *7*, 7632−7643.
(40) Tra, V. T.; Chen, J. W.; Huang, P. C.; Huang, B. C.; Cao, Y.; Yeh, C. H.; Liu, H.; Eliseev, E. A.; Morozovska, A. N.; Lin, J.; Chen, Y.; Chu, M. W.; Chiu, P.; Chiu, Y. P.; Chen, L.; Wu, C. L.; Chu, Y. Ferroelectric Control of the Conduction at the LaAlO3/SrTiO3 Heterointerface. *Adv. Mater.* **2013**, *25*, 3357−3336.
(41) Kaur, R.; Badea, I. Nanodiamonds as novel nanomaterials for biomedical applications: drug delivery and imaging systems. *Int. J. Nanomed.* **2013**, *8*, 203−220.
(42) Tang, F.; Li, L.; Chen, D. Mesoporous Silica Nanoparticles: Synthesis, Biocompatibility and Drug Delivery. *Adv. Mater.* **2012**, *24*, 1504−1534.
(43) Yang, P.; Gai, S.; Lin, J. Functionalized mesoporous silica materials for controlled drug delivery. *Chem. Soc. Rev.* **2012**, *41*, 3679−3698.
(44) Vallet-Regí, M.; Balas, F.; Arcos, D. Mesoporous Materials for Drug Delivery. *Angew. Chem., Int. Ed.* **2007**, *46*, 7548−7558.
(45) Wang, H.; Wang, K.; Tian, B.; Revia, R.; Mu, Q.; Jeon, M.; Chang, F.-C.; Zhang, M. Preloading of Hydrophobic Anticancer Drug into Multifunctional Nanocarrier for Multimodal Imaging, NIR-Responsive Drug Release, and Synergistic Therapy. *Small* **2016**, *12*, 6388−6397.
(46) Hudson, S. P.; Padera, R. F.; Langer, R.; Kohane, D. S. The biocompatibility of mesoporous silicates. *Biomaterials* **2008**, *29*, 4045−4055.
(47) Garcia-Bennett, B. F. A.; Fadeel, B. Better safe than sorry: Understanding the toxicological properties of inorganic nanoparticles manufactured for biomedical applications. *Adv. Drug Delivery Rev.* **2010**, *62*, 362−374.
(48) Wang, H.; Wang, K.; Mu, Q.; Stephen, R. Z.; Yu, Y.; Zhou, S.; Zhang, M. Mesoporous carbon nanoshells for high hydrophobic drug loading, multimodal optical imaging, controlled drug release, and synergistic therapy. *Nanoscale* **2017**, *9*, 1434−1442.
(49) Li, C.; Meng, Y.; Wang, S.; Qian, M.; Wang, J.; Lu, W.; Huang, R. Mesoporous Carbon Nanospheres Featured Fluorescent Aptasensor for Multiple Diagnosis of Cancer in Vitro and in Vivo. *ACS Nano* **2015**, *9*, 12096−12103.
(50) Qiao, Z. A.; Guo, B. K.; Binder, A. J.; Chen, J. H.; Veith, G. M.; Dai, S. Controlled Synthesis of Mesoporous Carbon Nanostructures via a "Silica-Assisted" Strategy. *Nano Lett.* **2013**, *13*, 207−212.
(51) Cheng, L.; Wang, C.; Feng, L.; Yang, K.; Liu, Z. Functional Nanomaterials for Phototherapies of Cancer. *Chem. Rev.* **2014**, *114*, 10869−10939.
(52) Hu, B.; Wang, K.; Wu, L.; Yu, S.-H.; Antonietti, M.; Titirici, M.-M. Engineering carbon materials from the hydrothermal carbonization process of biomass. *Adv. Mater.* **2010**, *22*, 813−828.
(53) Zhang, F.; Gu, D.; Yu, T.; Zhang, F.; Xie, S.; Zhang, L.; Deng, Y.; Wan, Y.; Tu, B.; Zhao, D. Mesoporous Carbon Single-Crystals from Organic-Organic Self-Assembly. *J. Am. Chem. Soc.* **2007**, *129*, 7746−7747.
(54) Jia, Q.; Ge, J.; Liu, W.; Liu, S.; Niu, G.; Guo, L.; Zhang, H.; Wang, P. Gold nanorod@silica-carbon dots as multifunctional phototheranostics for fluorescence and photoacoustic imaging-guided synergistic photodynamic/photothermal therapy. *Nanoscale* **2016**, *8*, 13067−13077.
(55) Lim, S. Y.; Shen, W.; Gao, Z. Carbon quantum dots and their applications. *Chem. Soc. Rev.* **2015**, *44*, 362−381.
(56) Guo, L.; Ge, J.; Liu, W.; Niu, G.; Jia, Q.; Wang, H.; Wang, P. Tunable multicolor carbon dots prepared from well-defined polythiophene derivatives and their emission mechanism. *Nanoscale* **2016**, *8*, 729−734.
(57) Du, Y.; Guo, S. Chemically doped fluorescent carbon and graphene quantum dots for bioimaging, sensor, catalytic and photoelectronic applications. *Nanoscale* **2016**, *8*, 2532−2543.
(58) Jiang, F.; Chen, D.; Li, R.; Wang, Y.; Zhang, G.; Li, S.; Zheng, J.; Huang, N.; Gu, Y.; Wang, C.; Shu, C. Eco-friendly synthesis of size-controllable amine-functionalized graphene quantum dots with antimycoplasma properties. *Nanoscale* **2013**, *5*, 1137−1142.
(59) Cao, L.; Wang, X.; Meziani, M. J.; Lu, F.; Wang, H.; Luo, P. G.; Lin, Y.; Harruff, B. A.; Veca, L. M.; Murray, D.; Xie, S.-Y.; Sun, Y.-P. Carbon Dots for Multiphoton Bioimaging. *J. Am. Chem. Soc.* **2007**, *129*, 11318−11319.
(60) Sun, Y.-P.; Zhou, B.; Lin, Y.; Wang, W.; Fernando, K. A. S.; Pathak, P.; Meziani, M. J.; Harruff, B. A.; Wang, X.; Wang, H.; Luo, P. G.; Yang, H.; Kose, M. E.; Chen, B.; Veca, L. M.; Xie, S.-Y. Quantum-Sized Carbon Dots for Bright and Colorful Photoluminescence. *J. Am. Chem. Soc.* **2006**, *128*, 7756−7757.
(61) Wang, Q.; Zheng, H.; Long, Y.; Zhang, L.; Gao, M.; Bai, W. Microwave−hydrothermal synthesis of fluorescent carbon dots from graphite oxide. *Carbon* **2011**, *49*, 3134−3140.
(62) Yang, S. T.; Wang, X.; Wang, H.; Lu, F.; Luo, P. G.; Cao, L.; Meziani, M. J.; Liu, J.-H.; Liu, Y.; Chen, M.; Huang, Y.; Sun, Y.-P. Carbon Dots as Nontoxic and High-Performance Fluorescence Imaging Agents. *J. Phys. Chem. C* **2009**, *113*, 18110−18114.
(63) Dahan, M.; Levi, S.; Luccardini, C.; Rostaing, P.; Riveau, B.; Triller, A. Diffusion dynamics of glycine receptors revealed by single-quantum dot tracking. *Science* **2003**, *302*, 442−445.
(64) Michalet, X.; Pinaud, F.; Bentolila, L. A.; Tsay, J. M.; Doose, S.; Li, J. J.; Sundaresan, G.; Wu, A. M.; Gambhir, S. S.; Weiss, S.

DOI: 10.1021/acsomega.8b01071
ACS Omega 2018, 3, 9126−9145

Quantum Dots for Live Cells, in Vivo Imaging, and Diagnostics. *Science* **2005**, *307*, 538−544.
(65) Farokhzad, O. C.; Cheng, J.; Teply, B. A.; Sherifi, I.; Jon, S.; Kantoff, P. W.; Richie, J. P.; Langer, R. Targeted nanoparticle-aptamer bioconjugates for cancer chemotherapy in vivo. *Proc. Natl. Acad. Sci. U. S. A.* **2006**, *103*, 6315−6320.
(66) Puzyr, A. P.; Pozdniakova, I. O.; Bondar, V. S. Design of a luminescent biochip with nanodiamonds and bacterial luciferase. *Phys. Solid State* **2004**, *46*, 761−763.
(67) Kaur, R.; Badea, I. Nanodiamonds as novel nanomaterials for biomedical applications: drug delivery and imaging systems. *Int. J. Nanomed.* **2013**, *8*, 203−220.
(68) Kossovsky, N.; Gelman, A.; Hnatyszyn, H. J.; Rajguru, S.; Garrell, R. L.; Torbati, S.; Freitas, S. S. F.; Chow, G.-M. Surface-modified diamond nanoparticles as antigen delivery vehicles. *Bioconjugate Chem.* **1995**, *6*, 507−511.
(69) Chang, Y. R.; Lee, H. Y.; Chen, K.; Chang, C. C.; Tsai, D. S.; Fu, C. C.; Lim, T. S.; Tzeng, Y. K.; Fang, C. Y.; Han, C. C.; Chang, H. C.; Fann, W. Mass production and dynamic imaging of fluorescent nanodiamonds. *Nat. Nanotechnol.* **2008**, *3*, 284−288.
(70) Chao, J. I.; Perevedentseva, E.; Chung, P. H.; Liu, K. K.; Cheng, C. Y.; Chang, C. C.; Cheng, C. L. Nanometer-sized diamond particle as a probe for biolabeling. *Biophys. J.* **2007**, *93*, 2199−2208.
(71) Gruber, A.; Drabenstedt, A.; Tietz, C.; Fleury, L.; Wrachtrup, J.; Von Borczyskowsky, C. Scanning Confocal Optical Microscopy and Magnetic Resonance on Single Defect Centers. *Science* **1997**, *276*, 2012−2014.
(72) Faklaris, O.; Joshi, V.; Irinopoulou, T.; Tauc, P.; Sennour, M.; Girard, H.; Gesset, C.; Arnault, J.-C.; Thorel, A.; Boudou, J.-P.; Curmi, P. A.; Treussart, F. Photoluminescent Diamond Nanoparticles for Cell Labeling: Study of the Uptake Mechanism in Mammalian Cells. *ACS Nano* **2009**, *3*, 3955−3962.
(73) Talapatra, S.; Ganesan, P. G.; Kim, T.; Vajtai, R.; Huang, M.; Shima, M.; Ramanath, G.; Srivastava, D.; Deevi, S. C.; Ajayan, P. M. Irradiationinduced magnetism in carbon nanostructures. *Phys. Rev. Lett.* **2005**, *95*, 097201.
(74) Chow, E. K.; Zhang, X. Q.; Chen, M.; Lam, R.; Robinson, E.; Huang, H.; Schaffer, D.; Osawa, E.; Goga, A.; Ho, D. Nanodiamond Therapeutic Delivery Agents Mediate Enhanced Chemoresistant Tumor Treatment. *Sci. Transl. Med.* **2011**, *3*, 73ra21.
(75) Schrand, A. M.; Lin, J. B.; Hens, S. C.; Hussain, S. M. Temporal and mechanistic tracking of cellular uptake dynamics with novel surface fluorophore-bound nanodiamonds. *Nanoscale* **2011**, *3*, 435−445.
(76) Chang, I. P.; Hwang, K. C.; Chiang, C.-S. Preparation of fluorescent magnetic nanodiamonds and cellular imaging. *J. Am. Chem. Soc.* **2008**, *130*, 15476−15481.
(77) Maitra, U.; Jain, A.; George, S. J.; Rao, C. N. R. Tunable fluorescence in chromophore functionalized nanodiamond induced by energy transfer. *Nanoscale* **2011**, *3*, 3192−3197.
(78) Zhang, Z.-Q.; Chen, M.; Lam, R.; Xu, X.; Osawa, E.; Ho, D. Polymer-functionalized nanodiamond platforms as vehicles for gene delivery. *ACS Nano* **2009**, *3*, 2609−2616.
(79) Alhaddad, A.; Adam, M.; Botsoa, J.; Dantelle, G.; Perruchas, S.; Gacoin, T.; Mansuy, C.; Lavielle, S.; Malvy, C.; Treussart, F.; Bertrand, J. Nanodiamond as a vector for siRNA delivery to ewing sarcoma cells. *Small* **2011**, *7*, 3087−3095.
(80) Tzeng, Y.-K.; Faklaris, O.; Chang, B.-M.; Kuo, Y.; Hsu, J.-H.; Chang, H.-C. Superresolution imaging of albumin-conjugated fluorescent nanodiamonds in cells by stimulated emission depletion. *Angew. Chem., Int. Ed.* **2011**, *50*, 2262−2265.
(81) Hartl, A.; Schmich, E.; Garrido, J. A.; Hernando, J.; Catharino, S.; Walter, S.; Feulner, P.; Kromka, A.; Steinmuller, D.; Stutzmann, M. Protein-modified nanocrystalline diamond thin films for biosensor applications. *Nat. Mater.* **2004**, *3*, 736−742.
(82) Chao, J.; Perevedentseva, E.; Chung, P. H.; Liu, K.; Cheng, C.; Chang, C.; Cheng, C. Nanometer-sized diamond particle as a probe for biolabeling. *Biophys. J.* **2007**, *93*, 2199−2208.
(83) Cheng, C.; Perevedentseva, E.; Tu, J. S.; Chung, P. H.; Cheng, C.; Liu, K.; Chao, J.; Chen, P.; Chang, C. Direct and in vitro observation of growth hormone receptor molecules in A549 human lung epithelial cells by nanodiamond labeling. *Appl. Phys. Lett.* **2007**, *90*, 163903.
(84) Huang, L.-C. L.; Chang, H.-C. Adsorption and immobilization of cytochrome c on nanodiamonds. *Langmuir* **2004**, *20*, 5879−5884.
(85) Nicolau, E.; Mendez, J.; Fonseca, J.; Griebenow, K.; Cabrera, C. R. Bioelectrochemistry of non-covalent immobilized alcohol dehydrogenase on oxidized diamond nanoparticles. *Bioelectrochemistry* **2012**, *85*, 1−6.
(86) Tran, D. T.; Vermeeren, V.; Grieten, L.; Wenmackers, S.; Wagner, P.; Pollet, J.; Janssen, K. P. F.; Michiels, L.; Lammertyn, J. Nanocrystalline diamond impedimetric aptasensor for the label-free detection of human IgE. *Biosens. Bioelectron.* **2011**, *26*, 2987−2993.
(87) Smith, A. H.; Robinson, E.; Zhang, X.; Chow, E. K.; Lin, Y.; Osawa, E.; Xi, J.; Ho, D. Triggered release of therapeutic antibodies from nanodiamond complexes. *Nanoscale* **2011**, *3*, 2844−2848.
(88) Liu, K. K.; Zheng, W. W.; Wang, C. C.; Chiu, Y. C.; Cheng, C. L.; Lo, Y. S.; Chen, C.; Chao, J. I. Covalent linkage of nanodiamond-paclitaxel for drug delivery and cancer therapy. *Nanotechnology* **2010**, *21*, 315106−315120.
(89) Barras, A.; Lyskawa, J.; Szunerits, S.; Woisel, P.; Boukherroub, R. Direct functionalization of nanodiamond particles using dopamine derivatives. *Langmuir* **2011**, *27*, 12451−12457.
(90) Lien, Z. Y.; Hsu, T. C.; Liu, K. K.; Liao, W. S.; Hwang, K. C.; Chao, J. I. Cancer cell labeling and tracking using fluorescent and magnetic nanodiamond. *Biomaterials* **2012**, *33*, 6172−6185.
(91) Shimkunas, R. A.; Robinson, E.; Lam, R.; Lu, S.; Xu, X.; Zhang, X. Q.; Huang, H.; Osawa, E.; Ho, D. Nanodiamond-insulin complexes as pH-dependent protein delivery vehicles. *Biomaterials* **2009**, *30*, 5720−5728.
(92) Kra tschmer, W.; Lamb, L. D.; Fostiropoulos, K.; Huffman, D. R. Solid C60: a new form of carbon. *Nature* **1990**, *347*, 354−358.
(93) Trpkovic, A.; Todorovic-Markovic, B.; Trajkovic, V. Toxicity of pristine versus functionalized fullerenes: mechanisms of cell damage and the role of oxidative stress. *Arch. Toxicol.* **2012**, *86*, 1809−1827.
(94) Tegos, G. P.; Demidova, T. N.; Arcila-Lopez, D.; Lee, H.; Wharton, T.; Gali, H.; Hamblin, M. R. Cationic fullerenes are effective and selective antimicrobial photosensitizers. *Chem. Biol.* **2005**, *12*, 1127−1135.
(95) Kroto, H. W.; Heath, J. R.; O'Brien, S. C.; Curl, R. F.; Smalley, R. E. C60:Buckminsterfullerene. *Nature* **1985**, *318*, 162−163.
(96) Piskoti, C.; Yarger, J.; Zettl, A. C36, a new carbon solid. *Nature* **1998**, *393*, 771−774.
(97) Guo, T.; Diener, M. D.; Chai, Y.; Alford, M. J.; Haufler, R. E.; McClure, S. M.; Ohno, T.; Weaver, J. H.; Scuseria, G. E.; Smalley, R. E. Uranium stabilization of C28: a tetravalent fullerene. *Science* **1992**, *257*, 1661−1664.
(98) Diederich, F.; Ettl, R.; Rubin, Y.; Whetten, R. L.; Beck, R.; Alvarez, M.; Anz, S.; Wudl, F.; Khemani, K. C.; Koch, A.; Sensharma, D. The higher fullerenes: isolation and characterization of C76, C84, C90, C94, and C70O, an oxide of D5 h-C70. *Science* **1991**, *252*, 548−551.
(99) Mroz, P.; Pawlak, A.; Satti, M.; Lee, H.; Wharton, T.; Gali, H.; Sarna, T.; Hamblin, M. R. Functionalized fullerenes mediate photodynamic killing of cancer cells: Type I versus Type II photochemical mechanism. *Free Radical Biol. Med.* **2007**, *43*, 711−719.
(100) Prat; Marti, C.; Nonell, S.; Zhang, X.; Foote, C. S.; Gonzalez Moreno, R.; Bourdelande, J. L.; Font, J. C60 Fullerene-based materials as singlet oxygen O2 (1Δg) photosensitizers: a time-resolved near-IR luminescence and optoacoustic study. *Phys. Chem. Chem. Phys.* **2001**, *3*, 1638−1643.
(101) Shi, J.; Wang, L.; Gao, J.; Liu, Y.; Zhang, J.; Ma, R.; Liu, R.; Zhang, Z. A fullerene-based multi-functional nanoplatform for cancer theranostic applications. *Biomaterials* **2014**, *35*, 5771−5784.
(102) Xiao, L.; Aoshima, H.; Saitoh, Y.; Miwa, N. The effect of squalane-dissolved fullerene-C60 on adipogenesis-accompanied oxi-

DOI: 10.1021/acsomega.8b01071
ACS Omega 2018, 3, 9126−9145

dative stress and macrophage activation in a preadipocyte-monocyte co-culture system. *Biomaterials* **2010**, *31*, 5976−5985.
(103) Zheng, X. T.; Ananthanarayanan, A.; Luo, K. Q.; Chen, P. Glowing graphene quantum dots and carbon dots: properties, syntheses, and biological applications. *Small* **2015**, *11*, 1620−1636.
(104) Zhu, S.; Zhou, N.; Hao, Z.; Maharjan, S.; Zhao, X.; Song, Y.; Sun, B.; Zhang, K.; Zhang, J.; Sun, H.; Lu, L.; Yang, B. Photoluminescent graphene quantum dots for bioimaging applications. *RSC Adv.* **2015**, *5*, 39399−39403.
(105) Zhu, S.; Zhang, J.; Qiao, C.; Tang, S.; Li, Y.; Yuan, W.; Li, B.; Tian, L.; Liu, F.; Hu, R.; Gao, H.; Wei, H.; Zhang, H.; Sun, H.; Yang, B. Strongly green-photoluminescent graphene quantum dots for bioimaging applications. *Chem. Commun.* **2011**, *47*, 6858−6860.
(106) Ge, J.; Lan, M.; Zhou, B.; Liu, W.; Guo, L.; Wang, H.; Jia, Q.; Niu, G.; Huang, X.; Zhou, H.; Meng, X.; Wang, P.; Lee, C.-S.; Zhang, W.; Han, X. A graphene quantum dot photodynamic therapy agent with high singlet oxygen generation. *Nat. Commun.* **2014**, *5*, 4596−4604.
(107) Kalluru, P.; Vankayala, R.; Chiang, C. S.; Hwang, K. C. Nano-graphene oxide-mediated In vivo fluorescence imaging and bimodal photodynamic and photothermal destruction of tumors. *Biomaterials* **2016**, *95*, 1−10.
(108) Gao, S.; Zhang, L.; Wang, G.; Yang, K.; Chen, M.; Tian, R.; Ma, Q.; Zhu, L. Hybrid graphene/Au activatable theranostic agent for multimodalities imaging guided enhanced photothermal therapy. *Biomaterials* **2016**, *79*, 36−45.
(109) Yang, L.; Liu, B.; Wang, M.; Li, J.; Pan, W.; Gao, X.; Li, N.; Tang, B. A Highly Sensitive Strategy for Fluorescence Imaging of MicroRNA in Living Cells and in Vivo Based on Graphene Oxide-Enhanced Signal Molecules Quenching of Molecular Beacon. *ACS Appl. Mater. Interfaces* **2018**, *10*, 6982−6990.
(110) Hu, S. H.; Chen, Y. W.; Hung, W. T.; Chen, I. W.; Chen, S. Y. Quantum-dot-tagged reduced graphene oxide nanocomposites for bright fluorescence bioimaging and photothermal therapy monitored in situ. *Adv. Mater.* **2012**, *24*, 1748−1754.
(111) Jensen, L.; Zhao, L. L.; Schatz, G. C. Size-Dependence of the Enhanced Raman Scattering of Pyridine Adsorbed on Agn (n = 2−8, 20) Clusters. *J. Phys. Chem. C* **2007**, *111*, 4756−4764.
(112) Liu, Q.; Wei, L.; Wang, J.; Peng, F.; Luo, D.; Cui, R.; Niu, Y.; Qin, X.; Liu, Y.; Sun, H.; Yang, J.; Li, Y. Cell imaging by graphene oxide based on surface enhanced Raman scattering. *Nanoscale* **2012**, *4*, 7084−7089.
(113) Gong, H.; Peng, R.; Liu, Z. Carbon nanotubes for biomedical imaging: the recent advances. *Adv. Drug Delivery Rev.* **2013**, *65*, 1951−1963.
(114) Campion, A.; Kambhampati, P. Surface Enhanced Raman Scattering. *Chem. Soc. Rev.* **1998**, *27*, 241−250.
(115) Weitz, D. A.; Garoff, S.; Gersten, J. I.; Nitzan, A. The enhancement of Raman scattering, resonance Raman scattering, and fluorescence from molecules adsorbed on a rough silver surface. *J. Chem. Phys.* **1983**, *78*, 5324−5338.
(116) Huang, J.; Zong, C.; Shen, H.; Liu, M.; Chen, B.; Ren, B.; Zhang, Z. Mechanism of cellular uptake of graphene oxide studied by surface-enhanced Raman spectroscopy. *Small* **2012**, *8*, 2577−2584.
(117) Zhang, C.-y.; Hao, R.; Zhao, B.; Hao, Y.-w.; Liu, Y.-q. A ternary functional Ag@GO@Au sandwiched hybrid as an ultra-sensitive and stable surface enhanced Raman scattering platform. *Appl. Surf. Sci.* **2017**, *409*, 306−313.
(118) Liu, Z.; Guo, Z.; Zhong, H.; Qin, X.; Wan, M.; Yang, B. Graphene oxide based surface-enhanced Raman scattering probes for cancer cell imaging. *Phys. Chem. Chem. Phys.* **2013**, *15*, 2961−2966.
(119) Chen, H.; Wang, Z.; Zong, S.; Wu, L.; Chen, P.; Zhu, D.; Wang, C.; Xu, S.; Cui, Y. SERS-fluorescence monitored drug release of a redox-responsive nanocarrier based on graphene oxide in tumor cells. *ACS Appl. Mater. Interfaces* **2014**, *6*, 17526−17533.
(120) Werner, E. J.; Datta, A.; Jocher, C. J.; Raymond, K. N. High-Relaxivity MRI Contrast Agents: Where Coordination Chemistry Meets Medical Imaging. *Angew. Chem., Int. Ed.* **2008**, *47*, 8568−8580.
(121) Wang, H.; Revia, R.; Wang, K.; Kant, R. J.; Mu, Q.; Gai, Z.; Hong, K.; Zhang, M. Paramagnetic Properties of Metal-Free Boron-Doped Graphene Quantum Dots and Their Application for Safe Magnetic Resonance Imaging. *Adv. Mater.* **2017**, *29*, 1605416.
(122) Wang, Y.; Huang, R.; Liang, G.; Zhang, Z.; Zhang, P.; Yu, S.; Kong, J. MRI-Visualized, dual-targeting, combined tumor therapy using magnetic graphene-based mesoporous silica. *Small* **2014**, *10*, 109−116.
(123) Zhang, M.; Cao, Y.; Chong, Y.; Ma, Y.; Zhang, H.; Deng, Z.; Hu, C.; Zhang, Z. Graphene oxide based theranostic platform for T1-weighted magnetic resonance imaging and drug delivery. *ACS Appl. Mater. Interfaces* **2013**, *5*, 13325−13332.
(124) Sun, C.; Lee, J. S.; Zhang, M. Magnetic nanoparticles in MR imaging and drug delivery. *Adv. Drug Delivery Rev.* **2008**, *60*, 1252−1265.
(125) Ai, H.; Flask, C.; Weinberg, B.; Shuai, X.-T.; Pagel, M. D.; Farrell, D.; Duerk, J.; Gao, J. Magnetite-Loaded Polymeric Micelles as Ultrasensitive Magnetic-Resonance Prebes. *Adv. Mater.* **2005**, *17*, 1949−1952.
(126) Rogers, W. J.; Basu, P. Factors regulating macrophage endocytosis of nanoparticles: implications for targeted magnetic resonance plaque imaging. *Atherosclerosis* **2005**, *178*, 67−73.
(127) Wang, G.; Chen, G.; Wei, Z.; Dong, X.; Qi, M. Multifunctional Fe3O4/graphene oxide nanocomposites for magnetic resonance imaging and drug delivery. *Mater. Chem. Phys.* **2013**, *141*, 997−1004.
(128) Wang, Y.; Huang, R.; Liang, G.; Zhang, Z.; Zhang, P.; Yu, S.; Kong, J. MRI-visualized, dual-targeting, combined tumor therapy using magnetic graphene-based mesoporous silica. *Small* **2014**, *10*, 109−116.
(129) Li, W.; Chen, X. Gold nanoparticles for photoacoustic imaging. *Nanomedicine* **2015**, *10*, 299−320.
(130) Ku, G.; Wang, X.; Stoica, G.; Wang, L. V. Multiple-bandwidth photoacoustic tomography. *Phys. Med. Biol.* **2004**, *49*, 1329−1338.
(131) Wang, X.; Pang, Y.; Ku, G.; Xie, X.; Stoica, G.; Wang, L. V. Noninvasive Laser-Induced Photoacoustic Tomography for Structural and Functional in Vivo Imaging of the Brain. *Nat. Biotechnol.* **2003**, *21*, 803−806.
(132) Qin, H.; Zhou, T.; Yang, S.; Xing, D. Fluorescence Quenching Nanoprobes Dedicated to In Vivo Photoacoustic Imaging and High-Efficient Tumor Therapy in Deep-Seated Tissue. *Small* **2015**, *11*, 2675−2686.
(133) Wang, L. H. V.; Hu, S. Photoacoustic Tomography: In Vivo Imaging from Organelles to Organs. *Science* **2012**, *335*, 1458−1462.
(134) Liu, Y.; Yang, X.; Huang, Z.; Huang, P.; Zhang, Y.; Deng, L.; Wang, Z.; Zhou, Z.; Liu, Y.; Kalish, H.; Khachab, N. M.; Chen, X.; Nie, Z. Magneto-Plasmonic Janus Vesicles for Magnetic Field-Enhanced Photoacoustic and Magnetic Resonance Imaging of Tumors. *Angew. Chem., Int. Ed.* **2016**, *55*, 15297−15300.
(135) Wang, P. H.; Liu, H. L.; Hsu, P. H.; Lin, C. Y.; Wang, C. C.-R.; Chen, P. Y.; Wei, K. C.; Yen, T. C.; Li, M. L. Gold-nanorod contrast-enhanced photoacoustic micro-imaging of focused-ultrasound induced blood-brain-barrier opening in a rat model. *J. Biomed. Opt.* **2012**, *17*, 061222.
(136) Chen, Y. S.; Frey, W.; Kim, S.; Kruizinga, P.; Homan, K.; Emelianov, S. Silica-Coated Gold Nanorods as Photoacoustic Signal Nanoamplifiers. *Nano Lett.* **2011**, *11*, 348−354.
(137) Moon, H.; Kumar, D.; Kim, H.; Sim, C.; Chang, J.-H.; Kim, J.-M.; Kim, H.; Lim, D.-K. Amplified photoacoustic performance and enhanced photothermal stability of reduced graphene oxide coated gold nanorods for sensitive photoacoustic imaging. *ACS Nano* **2015**, *9*, 2711−2719.
(138) Hu, D.; Zhang, J.; Gao, G.; Sheng, Z.; Cui, H.; Cai, L. Indocyanine Green-Loaded Polydopamine-Reduced Graphene Oxide Nanocomposites with Amplifying Photoacoustic and Photothermal Effects for Cancer Theranostics. *Theranostics* **2016**, *6*, 1043−1052.
(139) Massoud, T. F.; Gambhir, S. S. Molecular imaging in living subjects: seeing fundamental biological processes in a new light. *Genes Dev.* **2003**, *17*, 545−580.

DOI: 10.1021/acsomega.8b01071
ACS Omega 2018, 3, 9126−9145

(140) Gambhir, S. S. Molecular imaging of cancer with positron emission tomography. *Nat. Rev. Cancer* **2002**, *2*, 683−693.
(141) Garg, B.; Sung, C. H.; Ling, Y. C. Graphene-based nanomaterials as molecular imaging agents. *Wiley interdisciplinary reviews. Nanomedicine and nanobiotechnology* **2015**, *7*, 737−758.
(142) Wu, A. M. Engineered antibodies for molecular imaging of cancer. *Methods* **2014**, *65*, 139−147.
(143) Paudyal, B.; Zhang, K.; Chen, C. P.; Wampole, M. E.; Mehta, N.; Mitchell, E. P.; Gray, B. D.; Mattis, J. A.; Pak, K. Y.; Thakur, M. L.; Wickstrom, E. Determining efficacy of breast cancer therapy by PET imaging of HER2 mRNA. *Nucl. Med. Biol.* **2013**, *40*, 994−999.
(144) Marton, J.; Henriksen, G. Design and synthesis of an 18F-labeled version of phenylethyl orvinol ([18F]FE-PEO) for PET-imaging of opioid receptors. *Molecules* **2012**, *17*, 11554−11569.
(145) Veleva, A. N.; Nepal, D. B.; Frederick, C. B.; Schwab, J.; Lockyer, P.; Yuan, H.; Lalush, D. S.; Patterson, C. Efficient in vivo selection of a novel tumor-associated peptide from a phage display library. *Molecules* **2011**, *16*, 900−914.
(146) Chen, K.; Ma, W.; Li, G.; Wang, J.; Yang, W.; Yap, L. P.; Hughes, L. D.; Park, R.; Conti, P. S. Synthesis and evaluation of 64Cu-labeled monomeric and dimeric NGR peptides for microPET imaging of CD13 receptor expression. *Mol. Pharmaceutics* **2013**, *10*, 417−427.
(147) Lee, S.; Xie, J.; Chen, X. Peptide-based probes for targeted molecular imaging. *Biochemistry* **2010**, *49*, 1364−1376.
(148) Shao, Y.; Liang, W.; Kang, F.; Yang, W.; Ma, X.; Li, G.; Zong, S.; Chen, K.; Wang, J. 68Ga-labeled cyclic NGR peptide for microPET imaging of CD13 receptor expression. *Molecules* **2014**, *19*, 11600−11612.
(149) Deutscher, S. L. Phage display in molecular imaging and diagnosis of cancer. *Chem. Rev.* **2010**, *110*, 3196−3211.
(150) Chen, K.; Conti, P. S. Target-specific delivery of peptide-based probes for PET imaging. *Adv. Drug Delivery Rev.* **2010**, *62*, 1005−1022.
(151) Shi, S.; Yang, K.; Hong, H.; Valdovinos, H. F.; Nayak, T. R.; Zhang, Y.; Theuer, C. P.; Barnhart, T. E.; Liu, Z.; Cai, W. Tumor vasculature targeting and imaging in living mice with reduced graphene oxide. *Biomaterials* **2013**, *34*, 3002−3009.
(152) Yang, D.; Feng, L.; Dougherty, C. A.; Luker, K. E.; Chen, D.; Cauble, M. A.; Banaszak Holl, M. M.; Luker, G. D.; Ross, B. D.; Liu, Z.; Hong, H. In vivo targeting of metastatic breast cancer via tumor vasculature-specific nano-graphene oxide. *Biomaterials* **2016**, *104*, 361−371.
(153) Chen, L.; Zhong, X.; Yi, X.; Huang, M.; Ning, P.; Liu, T.; Ge, C.; Chai, Z.; Liu, Z.; Yang, K. Radionuclide (131)I labeled reduced graphene oxide for nuclear imaging guided combined radio- and photothermal therapy of cancer. *Biomaterials* **2015**, *66*, 21−28.
(154) Duan, S.; Yang, Y.; Zhang, C.; Zhao, N.; Xu, F. J. NIR-Responsive Polycationic Gatekeeper-Cloaked Hetero-Nanoparticles for Multimodal Imaging-Guided Triple-Combination Therapy of Cancer. *Small* **2017**, *13*, 1603133.
(155) Maes, F.; Collignon, A.; Vandermeulen, D.; Marchal, G.; Suetens, P. Multimodality image registration by maximization of mutual information. *IEEE Trans Med. Imaging* **1997**, *16*, 187−198.
(156) Liu, Z.; Dong, K.; Liu, J.; Han, X.; Ren, J.; Qu, X. Anti-biofouling polymer-decorated lutetium-based nanoparticulate contrast agents for in vivo high-resolution trimodal imaging. *Small* **2014**, *10*, 2429−2438.
(157) Yankeelov, T. E.; Abramson, R. G.; Quarles, C. C. Quantitative multimodality imaging in cancer research and therapy. *Nat. Rev. Clin. Oncol.* **2014**, *11*, 670−680.
(158) Sun, Y.; Zhu, X.; Peng, J.; Li, F. Core Shell Lanthanide Upconversion Nanophosphors as Four-Modal Probes for Tumor Angiogenesis Imaging. *ACS Nano* **2013**, *7*, 11290−11300.
(159) Zhang, Z.; Liu, Q.; Gao, D.; Luo, D.; Niu, Y.; Yang, J.; Li, Y. Graphene Oxide as a Multifunctional Platform for Raman and Fluorescence Imaging of Cells. *Small* **2015**, *11*, 3000−3005.
(160) Yang, K.; Hu, L.; Ma, X.; Ye, S.; Cheng, L.; Shi, X.; Li, C.; Li, Y.; Liu, Z. Multimodal imaging guided photothermal therapy using functionalized graphene nanosheets anchored with magnetic nanoparticles. *Adv. Mater.* **2012**, *24*, 1868−1872.
(161) Xu, C.; Shi, S.; Feng, L.; Chen, F.; Graves, S. A.; Ehlerding, E. B.; Goel, S.; Sun, H.; England, C. G.; Nickles, R. J.; Liu, Z.; Wang, T.; Cai, W. Long circulating reduced graphene oxide-iron oxide nanoparticles for efficient tumor targeting and multimodality imaging. *Nanoscale* **2016**, *8*, 12683−12692.
(162) Rong, P.; Yang, K.; Srivastan, A.; Kiesewetter, D. O.; Yue, X.; Wang, F.; Nie, L.; Bhirde, A.; Wang, Z.; Liu, Z.; Niu, G.; Wang, W.; Chen, X. Photosensitizer loaded nano-graphene for multimodality imaging guided tumor photodynamic therapy. *Theranostics* **2014**, *4*, 229−239.
(163) Jin, Y.; Wang, J.; Ke, H.; Wang, S.; Dai, Z. Graphene oxide modified PLA microcapsules containing gold nanoparticles for ultrasonic/CT bimodal imaging guided photothermal tumor therapy. *Biomaterials* **2013**, *34*, 4794−4802.
(164) Jakhmola, A.; Anton, N.; Vandamme, T. F. Inorganic Nanoparticles Based Contrast Agents for X-Ray Computed Tomography. *Adv. Healthcare Mater.* **2012**, *1*, 413−431.
(165) Wu, M.; Zhang, Y.; Zhang, Y.; Wu, M.; Wu, M.; Wu, H.; Cao, L.; Li, L.; Li, X.; Zhang, X. Tumor angiogenesis targeting and imaging using gold nanoparticle probe with directly conjugated cyclic NGR. *RSC Adv.* **2018**, *8*, 1706−1716.
(166) Xiao, Q.; Zheng, X.; Bu, W.; Ge, W.; Zhang, S.; Chen, F.; Xing, H.; Ren, Q.; Fan, W.; Zhao, K.; Hua, Y.; Shi, J. A Core/Satellite Multifunctional Nanotheranostic for in Vivo Imaging and Tumor Eradication by Radiation/Photothermal Synergistic Therapy. *J. Am. Chem. Soc.* **2013**, *135*, 13041−13048.
(167) Yi, H.; Ghosh, D.; Ham, M.-H.; Qi, J.; Barone, P. W.; Strano, M. S.; Belcher, A. M. M13 phage-functionalized single-walled carbon nanotubes as nanoprobes for second near-infrared window fluorescence imaging of targeted tumors. *Nano Lett.* **2012**, *12*, 1176−1183.
(168) Welsher, K.; Sherlock, S. P.; Dai, H. Deep-tissue anatomical imaging of mice using carbon nanotube fluorophores in the second near-infrared window. *Proc. Natl. Acad. Sci. U. S. A.* **2011**, *108*, 8943.
(169) Liang, C.; Diao, S.; Wang, C.; Gong, H.; Liu, T.; Hong, G.; Shi, X.; Dai, H.; Liu, Z. Tumor metastasis inhibition by imaging-guided photothermal therapy with single-walled carbon nanotubes. *Adv. Mater.* **2014**, *26*, 5646−5652.
(170) Welsher, K.; Liu, Z.; Daranciang, D.; Dai, H. Selective Probing and Imaging of Cells with Single Walled Carbon Nanotubes as Near-Infrared Fluorescent Molecules. *Nano Lett.* **2008**, *8*, 586−590.
(171) Lefebvre, J.; Austing, D. G.; Bond, J.; Finnie, P. Photoluminescence Imaging of Suspended Single-Walled Carbon Nanotubes. *Nano Lett.* **2006**, *6*, 1603−1608.
(172) Wang, F.; Dukovic, G.; Brus, L. E.; Heinz, T. F. The Optical Resonances in Carbon Nanotubes Arise from Excitons. *Science* **2005**, *308*, 838−841.
(173) Duque, J. G.; Pasquali, M.; Cognet, L.; Lounis, B. Environmental and synthesis-dependent luminescence properties of individual single-walled carbon nanotubes. *ACS Nano* **2009**, *3*, 2153−2156.
(174) Shi, D.; Guo, Y.; Dong, Z.; Lian, J.; Wang, W.; Liu, G.; Wang, L.; Ewing, R. C. Quantum-Dot-Activated Luminescent Carbon Nanotubes via a Nano Scale Surface Functionalization forin vivo Imaging. *Adv. Mater.* **2007**, *19*, 4033−4037.
(175) Nish, A.; Hwang, J. Y.; Doig, J.; Nicholas, R. J. Highly selective dispersion of single-walled carbon nanotubes using aromatic polymers. *Nat. Nanotechnol.* **2007**, *2*, 640−646.
(176) Dong, J.; Ye, Y.; Zhang, W.; Ren, Z.; Huo, Y.; Zheng, H. Preparation of Ag/Au bimetallic nanostructures and their application in surface-enhanced fluorescence. *Luminescence* **2015**, *30*, 1090−1093.
(177) Li, H.; Chen, C.-Y.; Wei, X.; Qiang, W.; Li, Z.; Cheng, Q.; Xu, D. Highly Sensitive Detection of Proteins based on Metal-Enhanced Fluorescence with Novel Silver Nanostructures. *Anal. Chem.* **2012**, *84*, 8656−8662.
(178) Camacho, S. A.; Sobral-Filho, R. G.; Aoki, P. H. B.; Constantino, C. J. L.; Brolo, A. G. Immunoassay quantification

DOI: 10.1021/acsomega.8b01071
ACS Omega 2018, 3, 9126−9145

using Surface-Enhanced Fluorescence (SEF) tags. *Analyst* **2017**, *142*, 2717−2724.
(179) Gersten, J.; Nitzan, A. Spectroscopic properties of molecules interacting with small dielectric particles. *J. Chem. Phys.* **1981**, *75*, 1139−1152.
(180) Anger, P.; Bharadwaj, P.; Novotny, L. Enhancement and quenching of single-molecule fluorescence. *Phys. Rev. Lett.* **2006**, *96*, 113002.
(181) Robinson, J. T.; Welsher, K.; Tabakman, S. M.; Sherlock, S. P.; Wang, H.; Luong, R.; Dai, H. High Performance In Vivo Near-IR (>1 mum) Imaging and Photothermal Cancer Therapy with Carbon Nanotubes. *Nano Res.* **2010**, *3*, 779−793.
(182) Welsher, K.; Liu, Z.; Sherlock, S. P.; Robinson, J. T.; Chen, Z.; Daranciang, D.; Dai, H. A route to brightly fluorescent carbon nanotubes for near-infrared imaging in mice. *Nat. Nanotechnol.* **2009**, *4*, 773−780.
(183) Harrison, B. S.; Atala, A. Carbon nanotube applications for tissue engineering. *Biomaterials* **2007**, *28*, 344−353.
(184) Kataura, H.; Kumazawa, Y.; Maniwa, Y.; Umezu, I.; Suzuki, S.; Ohtsuka, Y.; Achiba, Y. Optical Properties of Single-Wall Carbon Nanotubes. *Synth. Met.* **1999**, *103*, 2555.
(185) Hadjiev, V. G.; Arepalli, S.; Nikolaev, P.; Jandl, S.; Yowell, L. Enhanced Raman microprobe imaging of single-wall carbon nanotubes. *Nanotechnology* **2004**, *15*, 562−567.
(186) Heller, D. A.; Baik, S.; Eurell, T. E.; Strano, M. S. Single-Walled Carbon Nanotube Spectroscopy in Live Cells: Towards Long-Term Labels and Optical Sensors. *Adv. Mater.* **2005**, *17*, 2793−2799.
(187) Liu, Z.; Cai, W.; He, L.; Nakayama, N.; Chen, K.; Sun, X.; Chen, X.; Dai, H. In vivo biodistribution and highly efficient tumour targeting of carbon nanotubes in mice. *Nat. Nanotechnol.* **2007**, *2*, 47−52.
(188) Wang, X.; Wang, C.; Cheng, L.; Lee, S. T.; Liu, Z. Noble metal coated single-walled carbon nanotubes for applications in surface enhanced Raman scattering imaging and photothermal therapy. *J. Am. Chem. Soc.* **2012**, *134*, 7414−7422.
(189) Doan, B.-T.; Seguin, J.; Breton, M; Le Beherec, R.; Bessodes, M.; Rodriguez-Manzo, J. A.; Banhart, F.; Beloeil, J.-C.; Scherman, D.; Richard, C. Functionalized single-walled carbon nanotubes containing traces of iron as new negative MRI contrast agents for in vivo imaging. *Contrast Media Mol. Imaging* **2012**, *7*, 153−159.
(190) Tang, A. M.; Ananta, J. S.; Zhao, H.; Cisneros, B. T.; Lam, E. Y.; Wong, S. T.; Wilson, L. J.; Wong, K. K. Cellular uptake and imaging studies of gadolinium-loaded single-walled carbon nanotubes as MRI contrast agents. *Contrast Media Mol. Imaging* **2011**, *6*, 93−99.
(191) Sitharaman, B.; Kissell, K. R.; Hartman, K. B.; Tran, L. A.; Baikalov, A.; Rusakova, I.; Sun, Y.; Khant, H. A.; Ludtke, S. J.; Chiu, W.; Laus, S.; Toth, E.; Helm, L.; Merbach, A. E.; Wilson, L. J. Superparamagnetic gadonanotubes are high-performance MRI contrast agents. *Chem. Commun.* **2005**, *31*, 3915−3917.
(192) Holt, B. D.; Law, J. J.; Boyer, P. D.; Wilson, L. J.; Dahl, K. N.; Islam, M. F. Subcellular Partitioning and Analysis of Gd3+-Loaded Ultrashort Single-Walled Carbon Nanotubes. *ACS Appl. Mater. Interfaces* **2015**, *7*, 14593−14602.
(193) Ananta, J. S.; Godin, B.; Sethi, R.; Moriggi, L.; Liu, X.; Serda, R. E.; Krishnamurthy, R.; Muthupillai, R.; Bolskar, R. D.; Helm, L.; Ferrari, M.; Wilson, L. J.; Decuzzi, P. Geometrical confinement of gadolinium-based contrast agents in nanoporous particles enhances T1 contrast. *Nat. Nanotechnol.* **2010**, *5*, 815−821.
(194) Al Faraj, A.; Shaik, A. S.; Al Sayed, B. Preferential magnetic targeting of carbon nanotubes to cancer sites: noninvasive tracking using MRI in a murine breast cancer model. *Nanomedicine* **2015**, *10*, 931−948.
(195) Cisneros, B. T.; Law, J. J.; Matson, M. L.; Azhdarinia, A.; Sevick-Muraca, E. M.; Wilson, L. J. Stable confinement of positron emission tomography and magnetic resonance agents within carbon nanotubes for bimodal imaging. *Nanomedicine* **2014**, *9*, 2499−2509.
(196) Wang, C.; Ma, X.; Ye, S.; Cheng, L.; Yang, K.; Guo, L.; Li, C.; Li, Y.; Liu, Z. Protamine Functionalized Single-Walled Carbon Nanotubes for Stem Cell Labeling and In Vivo Raman/Magnetic Resonance/Photoacoustic Triple-Modal Imaging. *Adv. Funct. Mater.* **2012**, *22*, 2363−2375.
(197) Zhao, H.; Chao, Y.; Liu, J.; Huang, J.; Pan, J.; Guo, W.; Wu, J.; Sheng, M.; Yang, K.; Wang, J.; Liu, Z. Polydopamine Coated Single-Walled Carbon Nanotubes as a Versatile Platform with Radionuclide Labeling for Multimodal Tumor Imaging and Therapy. *Theranostics* **2016**, *6*, 1833−1843.
(198) Chen, Y.; Xu, P.; Wu, M.; Meng, Q.; Chen, H.; Shu, Z.; Wang, J.; Zhang, L.; Li, Y.; Shi, J. Colloidal RBC-shaped, hydrophilic, and hollow mesoporous carbon nanocapsules for highly efficient biomedical engineering. *Adv. Mater.* **2014**, *26*, 4294−4301.
(199) Zhou, L.; Jing, Y.; Liu, Y.; Liu, Z.; Gao, D.; Chen, H.; Song, W.; Wang, T.; Fang, X.; Qin, W.; Yuan, Z.; Dai, S.; Qiao, Z. A.; Wu, C. Mesoporous Carbon Nanospheres as a Multifunctional Carrier for Cancer Theranostics. *Theranostics* **2018**, *8*, 663−675.
(200) Zhang, J.; Zhang, J.; Li, W.; Chen, R.; Zhang, Z.; Zhang, W.; Tang, Y.; Chen, X.; Liu, G.; Lee, C. S. Degradable Hollow Mesoporous Silicon/Carbon Nanoparticles for Photoacoustic Imaging-Guided Highly Effective Chemo-Thermal Tumor Therapy in Vitro and in Vivo. *Theranostics* **2017**, *7*, 3007−3020.
(201) Shi, H.; Wei, J.; Qiang, L.; Chen, X.; Meng, X. Fluorescent carbon dots for biolmaging and biosensing applications. *J. Biomed. Nanotechnol.* **2014**, *10*, 2677−2699.
(202) Li, Y.; Zheng, X.; Zhang, X.; Liu, S.; Pei, Q.; Zheng, M.; Xie, Z. Porphyrin-based carbon dots for photodynamic therapy of hepatoma. *Adv. Healthcare Mater.* **2017**, *6*, 1600924.
(203) Liu, J. H.; Cao, L.; LeCroy, G. E.; Wang, P.; Meziani, M. J.; Dong, Y.; Liu, Y.; Luo, P. G.; Sun, Y. P. Carbon "Quantum" Dots for Fluorescence Labeling of Cells. *ACS Appl. Mater. Interfaces* **2015**, *7*, 19439−19445.
(204) Hong, G.; Diao, S.; Antaris, A. L.; Dai, H. Carbon nanomaterials for biological imaging and nanomedicinal therapy. *Chem. Rev.* **2015**, *115*, 10816−10906.
(205) Li, M.; Yu, C.; Hu, C.; Yang, W.; Zhao, C.; Wang, S.; Zhang, M.; Zhao, J.; Wang, X.; Qiu, J. Solvothermal conversion of coal into nitrogen-doped carbon dots with singlet oxygen generation and high quantum yield. *Chem. Eng. J.* **2017**, *320*, 570−575.
(206) Wang, J.; Qiu, J. A review of carbon dots in biological applications. *J. Mater. Sci.* **2016**, *51*, 4728−4738.
(207) Yang; Cao, S.-T.; Luo, L.; Lu, P. G.; Wang, F.; Wang, H.; Meziani, M. J.; Liu, Y.; Qi, G.; Sun, Y.-P. Carbon Dots for Optical Imaging in Vivo. *J. Am. Chem. Soc.* **2009**, *131*, 11308−11309.
(208) Zheng, M.; Ruan, S.; Liu, S.; Sun, T.; Qu, D.; Zhao, H.; Xie, Z.; Gao, H.; Jing, X.; Sun, Z. Self-Targeting Fluorescent Carbon Dots for Diagnosis of Brain Cancer Cells. *ACS Nano* **2015**, *9*, 11455−11461.
(209) Zhang, M.; Ju, H.; Zhang, L.; Sun, M.; Zhou, Z.; Dai, Z.; Zhang, L.; Gong, A.; Wu, C.; Du, F. Engineering iodine-doped carbon dots as dual-modal probes for fluorescence and X-ray CT imaging. *Int. J. Nanomed.* **2015**, *10*, 6943−6953.
(210) Zhang, Y.; Shen, Y.; Teng, X.; Yan, M.; Bi, H.; Morais, P. C. Mitochondria-targeting nanoplatform with fluorescent carbon dots for long time imaging and magnetic field-enhanced cellular uptake. *ACS Appl. Mater. Interfaces* **2015**, *7*, 10201−10212.
(211) Rondeau-Gagné, S.; Néabo, J. R.; Desroches, M.; Larouche, J.; Brisson, J.; Morin, J.-F. Topochemical Polymerization of Phenylacetylene Macrocycles: A New Strategy for the Preparation of Organic Nanorods. *J. Am. Chem. Soc.* **2013**, *135*, 110−113.
(212) Ge, J.; Jia, Q.; Liu, W.; Guo, L.; Liu, Q.; Lan, M.; Zhang, H.; Meng, X.; Wang, P. Red-Emissive Carbon Dots for Fluorescent, Photoacoustic, and Thermal Theranostics in Living Mice. *Adv. Mater.* **2015**, *27*, 4169−4177.
(213) Li, Y.; Zheng, X.; Zhang, X.; Liu, S.; Pei, Q.; Zheng, M.; Xie, Z. Porphyrin-Based Carbon Dots for Photodynamic Therapy of Hepatoma. *Adv. Healthcare Mater.* **2017**, *6*, 1600924.
(214) Jia, Q.; Zheng, X.; Ge, J.; Liu, W.; Ren, H.; Chen, S.; Wen, Y.; Zhang, H.; Wu, J.; Wang, P. Synthesis of carbon dots from Hypocrella bambusae for bimodel fluorescence/photoacoustic imaging-guided

DOI: 10.1021/acsomega.8b01071
ACS Omega 2018, 3, 9126−9145

synergistic photodynamic/photothermal therapy of cancer. *J. Colloid Interface Sci.* **2018**, *526*, 302−311.
(215) Ge, J.; Jia, Q.; Liu, W.; Lan, M.; Zhou, B.; Guo, L.; Zhou, H.; Zhang, H.; Wang, Y.; Gu, Y.; Meng, X.; Wang, P. Carbon Dots with Intrinsic Theranostic Properties for Bioimaging, Red-Light-Triggered Photodynamic/Photothermal Simultaneous Therapy In Vitro and In Vivo. *Adv. Healthcare Mater.* **2016**, *5*, 665−675.
(216) Nagl, A.; Hemelaar, S. R.; Schirhagl, R. Improving surface and defect center chemistry of fluorescent nanodiamonds for imaging purposes-a review. *Anal. Bioanal. Chem.* **2015**, *407*, 7521−7536.
(217) McGuinness, L. P.; Yan, Y.; Stacey, A.; Simpson, D. A.; Hall, L. T.; Maclaurin, D.; Prawer, S.; Mulvaney, P.; Wrachtrup, J.; Caruso, F.; Scholten, R. E.; Hollenberg, L. C. Quantum measurement and orientation tracking of fluorescent nanodiamonds inside living cells. *Nat. Nanotechnol.* **2011**, *6*, 358−363.
(218) Hou, W.; Toh, T. B.; Abdullah, L. N.; Yvonne, T. W. Z.; Lee, K. J.; Guenther, I.; Chow, E. K. Nanodiamond-Manganese dual mode MRI contrast agents for enhanced liver tumor detection. *Nanomedicine* **2017**, *13*, 783−793.
(219) Waddington, D. E. J.; Sarracanie, M.; Zhang, H.; Salameh, N.; Glenn, D. R.; Rej, E.; Gaebel, T.; Boele, T.; Walsworth, R. L.; Reilly, D. J.; Rosen, M. S. Nanodiamond-enhanced MRI via in situ hyperpolarization. *Nat. Commun.* **2017**, *8*, 15118.
(220) Lan, J.; Liu, C.; Gao, M.; Huang, C. An efficient solid-state synthesis of fluorescent surface carboxylated carbon dots derived from C60 as a label-free probe for iron ions in living cells. *Talanta* **2015**, *144*, 93−97.
(221) Kwag, D. S.; Park, K.; Oh, K. T.; Lee, E. S. Hyaluronated fullerenes with photoluminescent and antitumoral activity. *Chem. Commun.* **2013**, *49*, 282−284.
(222) Tan, L.; Wu, T.; Tang, Z. W.; Xiao, J. Y.; Zhuo, R. X.; Shi, B.; Liu, C. J. Water-soluble photoluminescent fullerene capped mesoporous silica for pH-responsive drug delivery and bioimaging. *Nanotechnology* **2016**, *27*, 315104.
(223) Li, T.; Murphy, S.; Kiselev, B.; Bakshi, K. S.; Zhang, J.; Eltahir, A.; Zhang, Y.; Chen, Y.; Zhu, J.; Davis, R. M.; Madsen, L. A.; Morris, J. R.; Karolyi, D. R.; Laconte, S. M.; Sheng, Z.; Dorn, H. C. A New Interleukin-13 Amino-Coated Gadolinium Metallofullerene Nanoparticle for Targeted MRI Detection of Glioblastoma Tumor Cells. *J. Am. Chem. Soc.* **2015**, *137*, 7881−7888.
(224) Chen, Z.; Ma, L.; Liu, Y.; Chen, C. Applications of functionalized fullerenes in tumor theranostics. *Theranostics* **2012**, *2*, 238−250.
(225) Zhen, M.; Zheng, J.; Wang, Y.; Shu, C.; Gao, F.; Zou, J.; Pyykko, I.; Wang, C. Multifunctional nanoprobe for MRI/optical dual-modality imaging and radical scavenging. *Chem. - Eur. J.* **2013**, *19*, 14675−14681.
(226) Han, Z.; Wu, X.; Roelle, S.; Chen, C.; Schiemann, W. P.; Lu, Z. R. Targeted gadofullerene for sensitive magnetic resonance imaging and risk-stratification of breast cancer. *Nat. Commun.* **2017**, *8*, 692.
(227) Wang, S.; Lin, J.; Wang, Z.; Zhou, Z.; Bai, R.; Lu, N.; Liu, Y.; Fu, X.; Jacobson, O.; Fan, W.; Qu, J.; Chen, S.; Wang, T.; Huang, P.; Chen, X. Core-Satellite Polydopamine-Gadolinium-Metallofullerene Nanotheranostics for Multimodal Imaging Guided Combination Cancer Therapy. *Adv. Mater.* **2017**, *29*, 1701013.
(228) Du, B.; Han, S.; Zhao, F.; Lim, K. H.; Xi, H.; Su, X.; Yao, H.; Zhou, J. A smart upconversion-based light-triggered polymer for synergetic chemo-photodynamic therapy and dual-modal MR/UCL imaging. *Nanomedicine* **2016**, *12*, 2071−2080.
(229) Shi, J.; Chen, Z.; Wang, L.; Wang, B.; Xu, L.; Hou, L.; Zhang, Z. A tumor-specific cleavable nanosystem of PEG-modified C60@Au hybrid aggregates for radio frequency-controlled release, hyperthermia, photodynamic therapy and X-ray imaging. *Acta Biomater.* **2016**, *29*, 282−297.

DOI: 10.1021/acsomega.8b01071
ACS Omega 2018, 3, 9126−9145